Pre-existing antibodies targeting a linear epitope on SARS-CoV-2 S2 cross-reacted with commensal gut bacteria and shaped vaccine induced immunity

Liqiu Jia[1, §], Shufeng Weng[2, §], Jing Wu[1, §], Xiangxiang Tian[3, 4], Yifan Zhang[3, 4], Xuyang Wang[1], Jing Wang[3, 5], Dongmei Yan[5], Wanhai Wang[4], Zhaoqin Zhu[3, #], Chao Qiu[6, #], Wenhong Zhang[1, 2, 7, 8, #], Ying Xu[2, #], Yanmin Wan[1, 2, 9, #]

[1] Department of Infectious Diseases, National Medical Center for Infectious Diseases, Shanghai Key Laboratory of Infectious Diseases and Biosafety Emergency Response, Huashan Hospital, Shanghai Medical College, Fudan University, Shanghai, China;
[2] State Key Laboratory of Genetic Engineering, Institute of Genetics, School of Life Science, Fudan University, Shanghai, China;
[3] Department of laboratory medicine, Shanghai Public Health Clinical Center, Shanghai, China;
[4] Clinical Laboratory, The First Affiliated Hospital of Zhengzhou University, Key Laboratory of Laboratory Medicine of Henan Province, Zhengzhou, Henan, P.R. China;
[5] Department of Immunology, School of Basic Medical, Jiamusi University, Jiamusi, Heilongjiang Province, China;
[6] Institutes of biomedical sciences & Shanghai Key Laboratory of Medical Epigenetics, Fudan University, Shanghai, China;
[7] National Clinical Research Center for Aging and Medicine, Huashan Hospital, Shanghai Medical College, Fudan University, Shanghai, China;
[8] Key Laboratory of Medical Molecular Virology (MOE/MOH) and Institutes of Biomedical Sciences, Shanghai Medical College, Fudan University, Shanghai, China.
[9] Department of radiology, Shanghai Public Health Clinical Center, Shanghai, China
[§] These authors contribute equally to this work.
[#] Correspondence should be addressed to: Zhaoqin Zhu, zhaoqinzhu@163.com; Chao Qiu, qiuchao@fudan.edu.cn; Wenhong Zhang, zhangwenhong@fudan.edu.cn; Ying Xu, yingxu2520@fudan.edu.cn; Yanmin Wan, yanmin_wan@fudan.edu.cn

Running title: SARS-CoV-2 antibody cross-reacts with gut bacteria

Word count: Abstract, 214; main text, 6208

Abstract

The origins of pre-existing SARS-CoV-2 cross-reactive antibodies and their potential impacts on vaccine efficacy have not been fully clarified. In this study, we demonstrated that S2 was the prevailing target of the pre-existing S protein cross-reactive antibodies in both healthy human and SPF mice. A dominant antibody epitope was identified on the connector domain of S2 (1147-SFKEELDKYFKNHT-1160, P144), which could be recognized by pre-existing antibodies in both human and mouse. Through metagenomic sequencing and fecal bacteria transplant, we proved that the generation of S2 cross-reactive antibodies was associated with commensal gut bacteria. Furthermore, six P144 specific monoclonal antibodies were isolated from mouse and proved to cross-react with commensal gut bacteria collected from both human and mouse. Mice with high levels of pre-existing S2 cross-reactive antibodies mounted higher S protein specific binding antibodies, especially against S2, after being immunized with a candidate COVID-19 DNA vaccine. Similarly, we found that levels of pre-existing antibodies against both S2 and P144 correlated positively with RBD specific binding antibody titers after two doses of inactivated SARS-CoV-2 vaccination in human. Taken together, our findings revealed that the pre-existing cross-reactive antibodies against SARS-CoV-2 spike protein could be induced by commensal gut bacteria and suggested that these pre-existing cross-reactive antibodies could facilitate the induction of S protein specific antibody responses after vaccination.

Key words: Cross-reactive antibody, SARS-CoV-2, Spike protein, commensal gut bacteria, vaccine immunogenicity

Introduction

Antibodies are vital components of the immune system that mediate protection against infections (1). When confronting infections, the actual role of pre-existing antibody depends on the following features (2): High titers of broadly neutralizing antibodies can protect the host against infection. While, when the pre-existing antibodies are non-neutralizing or with only a narrow neutralizing spectrum, hosts may not be sterilely protected or only be protected against specific serotypes of viruses. In addition to defending hosts against infections, pre-existing antibodies can also impact host immune responses upon infection or vaccination (3-5), which is best exemplified by the observations showing that pre-existing antibodies shaped the recall immune responses against influenza (6, 7).

For most occasions, pre-existing antibodies in adults derive from previous infection or vaccination except some “naturally” produced, poly-reactive antibodies (2, 8). When encountering a newly emerged or mutated virus, cross-reactive antibodies induced by previously occurred, phylogenetically closely related viruses constitute the main body of the pre-existing cross-reactive antibodies. The effect of this kind of pre-existing antibodies has been extensively investigated especially for infections of influenza (3, 7, 9) and flaviviruses (10-12). Of note, previous infection by phylogenetically similar viruses is not the sole source of pre-existing cross-reactive antibodies, as it has been clearly clarified that pre-existing antibodies against HIV-1 gp41 may stem from exposures to certain commensal gut bacteria (13-15). Besides, autoimmune diseases caused by cross-reactivities between microbial and self-antigens also implied that commensal gut bacteria represent important sources of cross-reactive antibodies (16-19).

Pre-existing antibodies against SARS-CoV-2 have also been observed in uninfected healthy individuals, which are speculated to be engendered by previous exposures to human common cold coronaviruses (20-26) or SARS-CoV (27-29). Meanwhile, sequence analyses (30) and a clinical observation (31) suggest that pre-existing SARS-CoV-2 antibodies might be engendered by common human pathogens and childhood vaccination. Although these two explanations are not mutually exclusive, they both need more experimental evidence to support.

In this study, we found that higher levels of SARS-CoV-2 S2 protein specific

antibodies existed in both healthy human and naïve SPF mice. To track the potential origins of these pre-existing cross-reactive antibodies, we mapped and located a dominant linear antibody epitope on S2, which could be recognized by pre-existing antibodies from both healthy human and naïve SPF mice. Monoclonal antibodies against this linear epitope were isolated from naïve SPF mice and proved to cross-react with commensal gut bacteria collected from both healthy human and naïve SPF mouse. Moreover, despite having been discussed iteratively (32, 33), the influences of pre-existing cross-reactive immunities on COVID-19 responses have not been clarified. Here we showed that high levels of pre-existing antibodies did not impair the immunogenicity of a candidate DNA vaccine encoding SARS-CoV-2 spike protein. On the contrary, mice with high levels of pre-existing antibodies mounted stronger S2 specific binding antibody responses compared with mice with low levels of pre-existing antibodies after immunization with a candidate DNA vaccine. Meanwhile, S1 specific T cell and binding antibody responses also tended to be stronger in mice with high levels of pre-existing antibodies, although no statistical significance was reached.

Results

Pre-existing antibodies recognizing a dominant linear epitope on SARS-CoV-2 S2 protein were detected in both human and mice

Pre-existing antibodies cross-react with SARS-CoV-2 S protein have been found in uninfected individuals by multiple previous studies (22, 25, 26, 34). It was postulated that the pre-existing immunities against SARS-CoV-2 might be induced by previous exposure to seasonal human coronaviruses (22, 30, 32, 33, 35). However, contradictive evidence suggested that human common cold coronavirus infection did not necessarily induce antibodies cross-reactive with SARS-CoV-2 spike protein (28, 36, 37). In addition to this hypothesis, an alternative explanation suggested that the cross-reactive immunities to SARS-CoV-2 might derive from other common human pathogens and vaccines (38).

To track the origins of the pre-existing cross-reactive antibodies to SARS-CoV-2 spike protein, in this study, we first measured the levels of pre-existing S protein specific antibodies in healthy human individuals and SPF mice. Our data showed that the cross-reactive antibody responses

against S2 were significantly stronger than those against S1 in plasma samples of healthy human collected both pre (2016 cohort) and post (2020 cohort) the outbreak of COVID-19 pandemic (Fig.1A and 1B). More strikingly, our data showed that binding antibodies targeting S2 could also be detected in two strains of naïve SPF mice (Fig. 1C and 1D). And this finding was further confirmed by Western-blotting (WB) assays, which showed that mouse sera with high ELISA-detected OD values (Fig. 2A) bound specifically with purified S2 while not S1 (Fig. 2B). Quite interestingly, the WB results indicated that cross-reactive antibodies against S2 also existed in the serum of a mouse (#487) with no detectable binding signal in the S2 ELISA assay (Fig. 2A and 2B). We next performed linear antibody epitope mapping using an in-house developed method of peptide competition ELISA. Our data showed that a single peptide (P144, aa1145-aa1162, 18 mer) accounted for most of the observed pre-existing antibody responses towards S2 in mice (Supplementary Figure 1). Via employing a series of truncated peptides based on P144, we determined the minimal range of this epitope (1147-SFKEELDKYFKNHT-1160), which locates on the connector domain (adjacent to the N-terminal of HR2 domain) (Fig. 2C). We also proved that antibodies recognizing this epitope widely existed in both healthy human and naïve SPF mice using the competitive ELISA assay (Fig.3).

The P144 specific antibody responses were engendered by exposures to certain commensal gut bacteria

To explore the potential origins of the pre-existed P144 specific antibodies, we first performed phylogenetic analyses among SARS-CoV-2 and other human coronaviruses. The results showed that the aa sequence of P144 was highly conserved among SARS-CoV-2 variants and SARS-CoV, while the similarities between P144 and MERS-CoV or seasonal human coronaviruses were relatively low, especially within the range of predicted antibody binding epitope (boxed fragment) (Supplementary Figure 2). The possibility of coronavirus infection in our SPF-mouse colonies was excluded by serum screening tests using commercialized mouse hepatitis virus (MHV) antigen and antibody detection kits (Data not shown).

Subsequently, to investigate whether environmental factors contribute to the induction of these S2 cross-reactive antibodies, we compared the levels of

pre-existing S2 binding antibodies between mice housed in SPF condition and mice maintained in a sterile isolation pack. Our data showed that the levels of pre-existing S2 binding antibodies were significantly higher in SPF mice (Figure 4A). Through metagenomic sequencing, we further demonstrated that the compositions of commensal gut bacteria were significantly different between mice housed in SPF condition and mice maintained in the sterile isolation pack (Supplementary Figure 3A). The abundance of bacteroidaceae, prevotellaceace and parabacteroides increased significantly in the commensal gut bacteria of SPF mice (Figure 4B). Moreover, flowcytometry assays indicated that the frequencies of S2 specific B cells ($CD3^{-}S2^{+}CD19^{+}$) in mesenteric lymph nodes were significantly higher than those in spleen (Supplementary Figure 3B). To further clarify the role of fecal microbiota in the induction of S2 cross-reactive antibodies, mice from isolation pack were transplanted with fecal bacteria prepared from SPF mice (Figure 4C). We found that P144 specific antibodies significantly increased after fecal microbiota transplantation (FMT) (Figure 4D). These results collectively suggested that the S2 cross-reactive antibodies might be induced by exposures to certain microbial antigens.

P144 specific monoclonal antibodies reacted with commensal gut bacteria from both human and mouse and showed limited neutralizing activities

To probe the potential antigens that might induce the P144 binding antibodies, we isolated 6 mAbs from two naïve SPF mice (one C57BL/6J mouse and one BALB/c mouse) with high levels of pre-existing S2 specific antibody responses. Five of these mAbs recognized P144 solely, while one mAb (clone M3) bound with P144 and P103 simultaneously (Supplementary Figure 4B). Results of competitive ELISA showed that the minimal epitopes varied slightly among the five P144 specific mAbs, especially at the C-terminal of P144 (Supplementary Figure 4A). The neutralizing potentials of these isolated monoclonal antibodies were evaluated using a pseudo virus-based neutralization assay. Our results showed that these monoclonal antibodies exhibited limited neutralizing activity against 5 major SARS-CoV-2 variants (Supplementary Figure 5). Of note, G18 neutralized the Indian strain (B.1.617) by 31%; F5 neutralized the UK strain (B.1.1.7) and the South African strain (B.1.351) by around 20%; G13

neutralized the South African strain (B.1.351) by nearly 20% (Supplementary Figure 5).

To prove the cross-reactivities between S2 and commensal gut microbial antigens, whole cell lysates (WCL) of mouse and human commensal gut bacteria were prepared and used as antigens for Western blotting assays, respectively. As shown in Figure 5A, specific bindings with the WCL of mixed fecal bacteria prepared from mice either with low levels of pre-existing antibodies (L) or with high levels of pre-existing antibodies (H) could be clearly visualized for each isolated mAbs. It was noteworthy that all mAbs except E10 strongly recognized a band around 180KD in the sample from mice with high pre-existing antibody responses. E10 predominantly recognized a band around 55KD in both samples, while stronger binding with the sample from mice with high pre-existing antibody responses could be visually observed (Figure 5A). Among the six mAbs, F5 showed the most diverse binding compacity. In addition to the band around 180KD, F5 bound with a band around 55KD (similar with E10) and a band between 40KD-55KD (Figure 5A). In comparison with the WB results of mouse samples, the recognized bands were less consistent across different human fecal bacteria samples (Figure 5B), presumably due to the individual to individual variation of gut microbiota composition. We found that a band around 70KD was recognized by most mAbs in 4 (lanes 1, 5, 6, 7) out of 7 samples and a band between 50KD-70KD was recognized by all mAbs in 3 (Lanes 2, 3, 7) out 7 samples. Besides, our data showed that the recognition pattern of each sample was largely consistent across different mAbs (Figure 5B).

Proteins corresponding to specifically recognized bands were excised from Coomassie blue stained gels and analyzed by the mass spectrometry. For the mouse fecal bacteria samples, protein bands with molecular weights around 180KD, 100KD, 55KD-70KD and 40KD-55KD (indicated by arrows in Figure 5A, panel F5) were selected. For human fecal bacteria samples, protein bands with molecular weights around 50KD-70KD, 70KD and 70KD-100KD (indicated by arrows in Figure 5B, panel F5) were selected. The lists of proteins identified in mouse and human samples were shown in Table 2 and Table 3, respectively. Proteins with molecular weights corresponding approximately to the excised protein bands were identified for both human and mouse fecal bacteria samples. Of note, multiple proteins within the theoretical

MW range of 58KD to 60KD were found to be identical between mouse and human samples, which included Fumarate hydratase class I (Accession# P14407), Formate-tetrahydrofolate ligase OS (Accession# Q189R2), Phosphoenolpyruvate carboxykinase (ATP) OS (Accession# C4ZBL1 and A6LFQ4) and 60 kDa chaperonin OS (Accession# A0Q2T1). To verify the cross-reactivity of the proteins detected by LC-MS, we selected E. coli (DH5α strain) as a representative target because *E. coli* derived Fumarate hydratase class I (Accession# P14407) were found in both human and mouse fecal bacteria samples. The result of WB assay showed that the P144 specific mAb (clone F5) recognized multiple bands with MWs consistent with *E. coli* proteins identified by LC-MS (Supplementary Figure 6).

Pre-existing S2 cross-reactive antibodies impacted specific immunities induced by a candidate COVID-19 DNA vaccine in mice

Pre-existing antibodies has been shown to be able to shape the recall immune responses upon influenza infection and vaccination (6). And the concern about how the pre-existing immunities may influence the effect of a SARS-CoV-2 vaccine has also attracted lots of attention (33). To investigate the impact of the pre-existing P144 antibodies on the immunogenicity of a candidate DNA vaccine, 18 BALB/c mice were divided into 3 groups according to their levels of pre-existing S2 binding antibodies and immunized with a DNA vaccine encoding the full length of SARS-CoV-2 S protein (Figure 6A and 6B). Our data showed that mice with high levels of pre-existing S2 binding antibodies mounted significantly higher S2 binding antibody responses after vaccination compared to mice with low or moderate levels of pre-existing S2 binding antibodies (Figure 6C). More specifically, the average level of P144 specific antibody responses was also stronger in mice with high levels of pre-existing S2 binding antibodies than mice with low levels of pre-existing S2 binding antibodies (Figure 6D and 6E). By comparison, both the S1 binding antibody and the neutralizing antibody titers did not significantly differ among all groups, despite that mice with moderate or high levels of pre-existing antibodies tended to mount higher average titer of S1 binding antibodies (Figure 6F and 6G). Mice without vaccination showed neither obvious S1 binding antibody response nor neutralizing activity (Data not shown). We further investigated the influence of pre-existing antibodies on humoral immune responses in

mouse respiratory tract after vaccination. And our data showed that the levels of S1 specific IgG in BALF were similar among the three groups after DNA vaccination (Figure 7A), while the average level of S2 specific IgG in BALF from mice with high pre-existing S2 binding antibodies was significantly higher than those from mice with low pre-existing antibodies (Figure 7B). S protein specific IgA response did not increase significantly after vaccination as compared with unvaccinated group (Figure 7C and 7D).

As most pre-existing antibodies in naïve SPF mice recognized P144 (Figure 2C and Supplementary Figure 1), we delineated the impact of pre-existing antibody on the epitope recognition after vaccination. Our results showed that the minimum epitope recognition pattern by the sera of mice with high levels of pre-existing antibodies remained unchanged after vaccination (Figure 8). Whereas the minimum epitope recognized by the sera of mice with moderate and low levels of pre-existing antibody responses altered at either the N-terminal or both terminals of P144 (Figure 8).

In addition to antibody measurement, we compared S protein specific T cell responses among the three groups as well (Figure 9A). The results showed that the candidate DNA vaccine elicited robust S protein specific T cell responses in all groups (Figure 9). Although no statistical significance was reached, interesting trends were observed: First, mice with high levels of pre-existing S2 binding antibodies tended to mount relatively higher S1 specific cellular immune responses (Figure 9B, 9C and 9D); second, as measured by the total responses of IL-6, IL-2 and TNF-a, mice with high levels of pre-existing antibodies tended to mount stronger T cell responses against S1 while lower responses against S2 (Figure 9C and 9D). Mice without vaccination showed no S protein specific T cells responses (Data not shown).

Pre-existing S2 cross-reactive antibodies correlated with RBD binding antibody responses after two-dose inactivated SARS-CoV-2 vaccination

To investigate how the pre-existing cross-reactive antibodies may influence the COVID-19 vaccine induced immunity, peripheral blood samples were collected from 28 healthy individuals who received two doses of an inactivated SARS-CoV-2 vaccine (Fig.10A). Correlation analyses showed that the levels of pre-existing P144 and S2 binding antibodies were significantly associated with RBD binding antibody titers at 14 days after immunization (Fig.10 B and

10E). Additionally, although not statistically significant, the pre-existing P144 binding antibody levels tended to correlate positively with neutralizing antibody responses after vaccination (P=0.0946) (Fig.10D).

Discussion

The origins of pre-existing cross-reactive immunities against SARS-CoV-2 have been investigated vigorously since the outbreak of the pandemic (39). Accumulating data suggest that cross-reactive T cells (33, 40-43) in SARS-CoV-2 unexposed human might be induced by previous infections of other hCoVs. While the origins of pre-existing cross-reactive antibodies could not be completely explained by previous infections of other coronaviruses, as recent studies revealed that the magnitude of antibody responses to SARS-CoV-2 S protein in the sera of patients with COVID-19 was not related to HCoVs' S titers (44) and immunization with coronaviruses OC43 did not induce significant SARS-CoV-2 S protein cross-reactive antibodies in mice. Moreover, it has also been observed that SARS-CoV-2 S protein specific binding antibody responses were weak in SARS-CoV-2 unexposed individuals with obvious binding antibody responses against S proteins of common cold hCoVs (45, 46).

To track the potential origins of the pre-existed cross-reactive antibodies targeting SARS-CoV-2 spike protein, in this study, we first screened the cross-reactive antibody responses in SARS-CoV-2 unexposed human plasma collected in 2020 and 2016, respectively. In both cohorts, we found that the magnitudes of S2 binding antibodies were significantly higher than those of S1 binding antibodies. This finding is consistent with previous studies showing that pre-existing S2 cross-reactive antibody responses are stronger than S1 cross-reactive antibody responses in SARS-CoV-2 unexposed individuals (44, 47, 48). Since S2 cross-reactive antibody responses have also been observed in unexposed animals (44), we continued to screen the cross-reactive antibody responses in two strains of naïve SPF mice. Our data showed that the OD values of S2 cross-reactive antibodies were significantly higher than those of S1 cross-reactive antibodies in naïve BALB/c and C57BL/6 mice. Detections of mouse sera collected from another two independent SPF animal facilities confirmed this finding (Data not shown). We also tried to detect the SARS-CoV-2 S protein specific T cells responses in mice with high

pre-existing S2 cross-reactive antibodies using the IFN-γ ELISPOT assay, which showed that there was no pre-existing cross-reactive T cell response.

To facilitate the search of potential antigens that induced the cross-reactive antibodies, we identified a dominant antibody epitope (P144) through a method of competitive ELISA based linear antibody epitope mapping. P144 is located within the connector domain of S2 (aa1147-aa1160, directly N-terminal of the HR2 region). The same epitope has been predicted (38) and detected in both SARS-CoV-2 unexposed and infected individuals by multiple previous studies (22, 23, 25, 26, 32). In this study, we also detected P144 specific antibody responses in plasma of healthy individuals collected in both 2020 and 2016. More interestingly, we found that the pre-existing S2 cross-reactive antibodies in mice were predominantly against the single epitope. Of note, although the aa sequence of P144 is highly conserved between SARS-CoV-2 and SARS-CoV, its similarity with four seasonal hCoVs is relatively low. A recent study showed that this epitope was more frequently recognized than its homologous peptides from common cold hCoVs by antibodies in plasma of COVID-19 negative individuals (23). The above evidence implied again that the pre-existing S2 specific antibodies might not be necessarily elicited by previous common cold coronavirus infections.

As the pre-existing S2 binding antibodies in mice were predominantly against P144, it provided us a good chance to unveil their origins. To do so, we first labeled mouse B cells with purified S2 protein and found that the frequency of S2 specific B cells was significantly higher in mesenteric LN than in spleen, suggesting that the gastrointestinal tract might be the primary site where the cross-reactive B cells were activated. Exposure to a certain gut microbial antigen, which can promote B cell diversification and stimulate antibody production in both T-dependent and -independent ways (49), might account for the presence of the cross-reactive antibodies. To prove this hypothesis, we next compared the levels of pre-existing S2 cross-reactive antibodies between mice housed in a sterile isolation pack and mice maintained in SPF condition. Our results showed that the levels of pre-existing S2 cross-reactive antibodies were significantly higher in SPF mice. Through metagenomic sequencing, we further demonstrated that the abundance of bacteroidaceae, prevotellaceace and parabacteroides were also significantly higher in the commensal gut bacteria of SPF mice. Moreover, we found that transplantation of fecal

microbiota from SPF mice could induce P144 cross reactive antibodies in mice bred in the isolation pack. These evidences suggested that the S2 cross-reactive antibodies could be induced by certain commensal gut bacteria. To identify the potential cross-reactive bacterial antigens, we isolated six P144 specific monoclonal antibodies from a naïve BALB/c mouse and a naïve C57BL/6 mouse, respectively. All the six mAbs were confirmed to be able to bind with P144 and showed weak neutralizing compacities against five SARS-CoV-2 variants. Leveraging these mAbs, we detected the cross-reactive antigens in mouse and human fecal microbiota through WB assays. Compared with a control mouse IgG, specific bands were observed for each mAb, which proved the antibody cross-reactivities between SARS-CoV-2 and commensal gut bacteria. The strongly recognized protein bands were further analyzed by LC-MS. Our data showed that cross-reactive antigens derived from bacteroides and parabacteroides were frequently identified in fecal bacteria samples of both human and mouse, which was consistent with our metagenomic sequencing data showing that the abundance of bacteroides and parabacteroides was significantly higher in the commensal gut bacteria of mice with high pre-existing S2 binding antibody levels. More intriguingly, five cross-reactive microbial antigens were identified in mouse and human fecal samples simultaneously, which implied that the S2 cross-reactive antibodies might naturally occur in different species of mammals. We also analyzed the sequence similarities between P144 and the proteins identified by LC-MS. Our results showed that most identified proteins shared varied identities with P144 (40%-70%, for more than 8 residues) (Data not shown). The cross-reactive epitopes on the identified proteins could not be specified based on our current data. Besides, the neutralizing mechanism(s) of P144 specific antibodies and their potential influences on gut microbiota were not clarified in this study. We plan to look into these issues in future.

In parallel with tracking the initial antigens that induced the S2 cross-reactive antibodies, we investigated the impact of pre-existing antibodies on the immunogenicity of a candidate DNA vaccine as well. According to previous reports, pre-existing cross-reactive antibodies may influence the effects of different vaccines differentially (6, 50). In this study, we found that the pre-existing cross-reactive antibodies shaped the vaccine-induced immune responses in both mouse and human. Mice with high levels of pre-existing

antibodies mounted stronger S2 binding antibodies in both peripheral blood and bronchial lavage after vaccination. More interestingly, we found that the pre-existing antibody levels correlated positively with post-vaccination RBD binding antibody titers in human. These findings proved that the pre-existing S2 binding antibodies could facilitate the generation of vaccine induced antibody responses. Through epitope mapping, we observed that the pre-existing antibodies strongly restricted the minimal epitope recognition in mice with high levels of pre-existing antibodies, which suggested that the imprint effect of pre-existing cross-reactive antibodies on vaccine induced antibody responses was primarily epitope specific. In addition to antibody response, we also found that the high levels of pre-existed S2 binding antibodies tended to induce higher S1 specific T cell responses while lower S2 specific T cell responses, implying that the pre-existing antibodies might change the balance between humoral versus cellular immune responses against the cross-reactive antigen. Since we did not perform the live virus challenge, it is still not clear how the pre-existing cross-reactive antibodies will impact vaccine efficacy *in vivo*. Nonetheless, as both our results and a recently published study suggested that antibodies targeting P144 epitope could neutralize SARS-CoV-2(51), we speculate that the pre-existing P144 cross-reactive antibodies may have protective effect.

A deep understanding of pre-existing cross-reactive antibodies against SARS-CoV-2 will enable better therapeutic, diagnostic and vaccine strategies. In this study, we provided evidence showing that antibodies targeting a conserved linear epitope on S2 cross-reacted with gut microbial antigens from both human and mouse, manifesting that some of the pre-existing cross-reactive antibodies might be induced by exposure to certain commensal gut bacteria. We proved that the pre-existing S2 cross-reactive antibodies did not impair the immunogenicity of a candidate DNA vaccine in a mouse model. Further investigations into the role of P144 specific antibody after SARS-CoV-2 infection and its impact on gut microbiota might provide clues to elucidate the mechanisms underlying the gastrointestinal symptom of COVID-19 (52-54).

Materials and methods

Ethics statement

All experiments and methods were performed in accordance with relevant guidelines and regulations. Experiments using mice and samples of healthy human were approved by the Research Ethics Review Committee of the Shanghai Public Health Clinical Center Affiliated to Fudan University. The study involving 28 healthy vaccinees was reviewed and approved by the institutional ethics committee of Hubei provincial CDC, China.

Plasma samples of healthy human

Two batches of plasma samples were collected from healthy individuals at the health screening clinic of Shanghai Public Health Clinical Center. A concurrent batch was collected in December 2020. All the 95 individuals enrolled in this batch reported no epidemiological link with confirmed COVID-19 patients and were confirmed to be free from any chronic or acute disease. Viral RNA tests confirmed that all individuals in this batch were free from SARS-CoV-2 infection. In addition, a historical batch of 78 plasma samples from healthy individual cohort (collected in 2016) were also measured for their cross reactivities with SARS-CoV-2 S protein. Demographical information about these two cohorts was described in Table 1.

Detection of SARS-CoV-2 S1 and S2 specific binding antibodies

In-house enzyme-linked immunosorbent assays (ELISA) were developed to measure SARS-CoV-2 S1 and S2 specific binding antibodies. High-binding 96-well EIA plates (Cat# 9018, Corning, USA) were coated with purified SARS-CoV-2 S1 (Cat# 40591-V08H, Sino Biological, China) or S2 proteins (Cat# 40590-V08B, Sino Biological, China) at a final concentration of 1μg/ml in carbonate/bi-carbonate coating buffer (30mM $NaHCO_3$,10mM Na_2CO_3, pH 9.6). Subsequently, the plates were blocked with 1×PBS containing 5% milk for 1 hour at 37°C. Next, 100μl of diluted human plasma or mouse serum was added to each well. After 1-hour incubation at 37°C, the plates were washed with 1×PBS containing 0.05% Tween20 for 5 times. Then, 100μl of a HRP labeled goat anti-mouse IgG antibody (Cat# ab6759, Abcam, UK) or goat anti-mouse IgG antibody (Cat# 115-035-003, Jackson Immuno Research, USA) diluted in 1×PBS containing 5% milk were added to each well and incubated for 1 hour at 37°C. After a second round of wash, 100μl of TMB substrate reagent (Cat# MG882, MESGEN, China) was added to each well. 15 minutes

later, the color development was stopped by adding 100μl of 1M H_2SO_4 to each well and the values of optical density at $OD450_{nm}$ and $OD630_{nm}$ were measured using 800 TS microplate reader (Cat# 800TS, Biotek, USA).

Competitive ELISA

According to the reference sequence of SARS-CoV-2 (Genebank accession number: NC_045512), peptides (18-mer overlapping by 11 residues, purities > 95%) encompass the full length of S protein were synthesized by GL Biochem (Shanghai, China). The experiment procedure was generally similar with the afore mentioned in-house ELISA assays, except that the diluted mouse serum or human plasma were incubated with synthesized peptides (5μg/ml) for 1 hour at room temperature before adding into the coated EIA plates. 1×PBS containing 0.01% DMSO (the solvent used to dissolve peptides) were used as the negative control in this assay.

Antibody avidity assay

Avidity of Ag-specific Ab was determined by ELISA as reported (55) with minor modifications. Briefly, plates were coated as the regular ELISA assay described above. Diluted (1:200) mouse sera were added into each well. After 1-hour incubation, ELISA plates were washed with washing buffer and incubated with 1.5M NaSCN or PBS for 15 mins at room temperature and then immediately washed with washing buffer. Ab avidity index was defined as the ratio of the OD value of a sample with 1.5M NaSCN treatment versus the OD value of the same sample with PBS treatment.

FACS analysis of S2 specific B cells in mice

Spleen and mesenteric lymph nodes were isolated from naïve SPF mice and single-cell suspensions were freshly prepared. After counting, 1×10^6 single cells were resuspended in 100μl R10 (RPMI1640 containing 10% fatal bovine serum) and incubated with biotinylated S2 protein (Cat# 40590-V08B-B, Sino Biological, China) for 30 minutes at room temperature. After incubation, the cells were washed twice with 500μl R10. Then, the cells were incubated with the mixture of PE-anti-mouse CD19 (Cat# 152408, Biolegend, USA, 1μl/test), BV510-anti-mouse CD45 (Cat# 103137, Biolegend, USA, 1.25μl/test) and Streptavidin-IF647 (Cat# 46006, AAT Bioquest, USA, 0.2μl/test) at room

temperature for 30 minutes. After washing, the stained cells were resuspended in 200μl 1×PBS and analyzed using a BD LSRFortessa™ Flow Cytometer. The data were analyzed using the FlowJo software (BD Biosciences, USA).

Preparation of P144 specific monoclonal antibodies

Monoclonal antibodies against P144 were prepared from one naïve BALB/c mouse and one naïve C57BL/6 mouse respectively using the hybridoma technique. Briefly, freshly isolated splenocytes were mixed and fused with SP2/0 cells at a ratio of 1:10. Hybridoma cell clones secreting P144 specific antibodies were screened by ELISA and monoclonal hybridoma cells were selected by multiple rounds of limited dilution. Selected clones of hybridoma cells were injected intraperitoneally into BALB/c×ICR hybrid mice. About 1-2 weeks later, peritoneal fluid was collected, and monoclonal IgG was purified using Protein A resin. The purities of monoclonal antibodies were verified using SDS-PAGE and the antibody concentrations were determined using a BCA kit (Cat# P0012, Beyotime Biotechnology, China).

Isolation of gut commensal bacteria and preparation of whole cell lysate (WCL)

About 2g of each fecal sample was suspended with 15ml sterile 1×PBS and vortexed thoroughly to obtain uniform mixtures. After centrifugation at 200×g for 5 min, the supernatants were collected, and the sediments were discarded. This process was repeated twice. Next, all the supernatant samples were centrifuged twice at 9000×g for 5 min and the supernatants were discarded. The precipitated bacteria pellets were resuspended in 500μl of 1×PBS (containing 1mM PMSF) and disrupted with an ultrasonic cell crusher (the probe-type sonicator, Model JY92-II; Ningbo Scientz Biotechnology Co., Ltd, China). After sonication, the samples were centrifuged at 10000rpm for 30 minutes to remove the cellular debris.

Western blotting

WCL containing 10μg of total protein was separated by SDS-PAGE (10% acrylamide gels) and then transferred onto a PVDF membrane (Cat# IPVH00010, Millipore, USA) or stained with Coomassie brilliant blue. After blocking with 5% skim milk for 2h, the membrane was incubated with a P144

specific monoclonal antibody or a control mouse IgG at a concentration of 1 µg/ml. After washing, the membrane was incubated with HRP conjugated goat anti-mouse IgG antibody (Cat # ab6759, Abcam, UK) diluted 1:5000 in TBST (Tris-buffered saline, pH 8.0, 0.05% Tween 20) containing 5% skim milk. After wash, the bands were developed with an ultra-sensitive ECL substrate (Cat# K-12045-D10, Advansta, USA). The area corresponding to the specific WB bands were excised from the gel stained with Coomassie blue and analyzed using the mass spectrometry.

Mass spectrometry analysis

The FASP digestion was adapted for the following procedures in Microcon PL-10 filters. After three-time buffer displacement with 8 M Urea and 100 mM Tris-HCl, pH 8.5, proteins were reduced by 10 mM DTT at 37 °C for 30 min and followed by alkylation with 30 mM iodoacetamide at 25°C for 45 min in dark. Digestion was carried out with trypsin (enzyme/protein as 1:50) at 37°C for 12 h after a wash with 20% ACN and three-time buffer displacement with digestion buffer (30 mM Tris-HCl, pH 8.0). After digestion, the solution was filtrated out and the filter was washed twice with 15% ACN, and all filtrates were pooled and vacuum-dried to reach a final concentration to 1 mg/ml. LC-MS analysis was performed using a nanoflow EASYnLC 1200 system (Thermo Fisher Scientific, Odense, Denmark) coupled to an Orbitrap Fusion Lumos mass spectrometer (Thermo Fisher Scientific, Bremen, Germany). A one-column system was adopted for all analyses. Samples were analyzed on a home-made C18 analytical column (75 µm i.d. × 25 cm, ReproSil-Pur 120 C18-AQ, 1.9 µm (Dr. Maisch GmbH, Germany)). The mobile phases consisted of Solution A (0.1% formic acid) and Solution B (0.1% formic acid in 80% ACN). The derivatized peptides were eluted using the following gradients: 2–5% B in 2 min, 5–35% B in 100 min, 35–44% B in 6 min, 44–100% B in 3 min, 100% B for 10 min, at a flow rate of 200 nl/min. Data-dependent analysis was employed in MS analysis: The time between master scan was 3s, and fragmented in HCD mode, normalized collision energy was 30.

Construction and preparation of a candidate DNA vaccine encoding SARS-CoV-2 full length S protein

The full-length *s* gene sequence of the reference SARS-CoV-2 strain was

591 optimized according to the preference of human codon usage and synthesized
592 by GENEWIZ life science company (Suchow, China). The codon optimized
593 spike gene was subcloned into a eukaryotic expression vector (pJW4303,
594 kindly gifted by Dr. Shan Lu's Laboratory at the University of Massachusetts)
595 (56). And the sequence of inserted gene was verified by Sanger sequencing
596 (Sangon Biotech Co., Ltd., Shanghai, China). An EndoFree Plasmid
597 Purification Kit (Cat#12391, Qiagen, Hilden, USA) was used to prepare the
598 recombinant plasmid for mouse vaccination.
599
600 **Mouse vaccination**
601 Peripheral blood samples were collected from female adult mice and
602 pre-existing S2 binding antibodies were measured using the previously
603 described in-house ELISA method. According to their pre-existing S2 binding
604 antibody levels (at 1:100 dilution of serum), the mice were divided into three
605 groups: low ($0.015 < OD_{450nm-630nm} \leqslant 0.130$, n=6), moderate ($0.130 <$
606 $OD_{450nm-630nm} \leqslant 0.750$, n=6) and high ($OD_{450nm-630nm} > 0.750$, n=6). All mice
607 were immunized intramuscularly with the candidate S protein DNA vaccine
608 (50μg/mouse) for three times at an interval of 2 weeks. Three weeks post the
609 third vaccination, the mice were euthanized. Peripheral blood, bronchial lavage
610 and spleen were collected for assays of S protein specific immune responses.
611
612 **Metagenomic analysis of mouse gut microbiota**
613 Stool (fecal) samples were self-collected and DNA was extracted from 250 mg
614 of each fecal sample in duplicate. The DNA samples were separated strictly
615 according to TIANamp Stool DNA Kit (Cat# DP328, TIANGEN, China). Then, a
616 total amount of 1μg DNA per sample was used as input material for the DNA
617 sample preparations. Sequencing libraries were generated using NEBNext®
618 Ultra™ DNA Library Prep Kit for Illumina (NEB, USA) following manufacturer's
619 recommendations and index codes were added to attribute sequences to each
620 sample. Briefly, the DNA sample was fragmented by sonication to a size of
621 350bp, then DNA fragments were end-polished, A-tailed, and ligated with the
622 full-length adaptor for Illumina sequencing with further PCR amplification. At
623 last, PCR products were purified (AMPure XP system) and libraries were
624 analyzed for size distribution by Agilent 2100 Bioanalyzer and quantified using
625 real-time PCR. The clustering of the index-coded samples was performed on a

cBot Cluster Generation System according to the manufacturer's instructions. After cluster generation, the library preparations were sequenced on an Illumina Novaseq 6000 platform and paired-end reads were generated.

SARS-CoV-2 pseudo-virus neutralization assay

VSV-backboned SARS-CoV-2 pseudo-viruses were prepared according to a reported method (57). The neutralization assay was conducted by following the previously described procedure (57, 58). Briefly, 100μl of serially diluted mice sera were added into 96-well cell culture plates. Then, 50μl of pseudo-viruses with a titer of 13000 $TCID_{50}$/ml were added into each well and the plates were incubated at 37°C for 1 hour. Next, Vero cells were added into each well (2×10^4 cells/well) and the plates were incubated at 37°C in a humidified incubator with 5% CO_2. 24 hours later, luminescence detection reagent (Bright-Glo™ Luciferase Assay System, Promega, USA) was added to each well following the manufacturer`s instruction. The luminescence was measured using a luminescence microplate reader (GloMax® Navigator Microplate Luminometer, Promega, USA) within 5 minutes. The Reed-Muench method was used to calculate the virus neutralization titer. Antibody neutralization titers were presented as 50% maximal inhibitory concentration (IC_{50}).

Detections of S protein specific cellular immune responses

SARS-CoV-2 S protein specific IFN-γ releases were measured using the method of enzyme-linked immunosorbent spot (ELISPOT) assays (Cat# 551083, BD Bioscience, USA) according to a previously described procedure (59). Briefly, the 96-well ELISPOT plates were coated with purified anti-mouse IFN-γ monoclonal antibody overnight at 4°C. Then, the plates were blocked and 2×10^5 fresh splenocytes were added into each well and incubated with peptide pools for 20 hours at 37°C in a humidified incubator with 5% CO_2. The final concentration for each peptide was 1μg/ml. After incubation, detecting antibody and Avidin-HRP were added sequentially. Finally, the plates were developed using the BD™ ELISPOT AEC Substrate Set (Cat#551951, BD Bioscience, USA) according to the manufacturer's manual. Spots representing IFN-γ producing cells were enumerated using an automated ELISPOT plate reader (ChampSpot III Elispot Reader, Saizhi, Beijing, China). At the same

time, the supernatants in the wells of ELISPOT plates were also collected for detecting secreted cytokines using a multiplexed cytokine beads array kit (Cat# 741054, Biolegend, USA).

Statistical analysis

All statistical analyses were performed using GraphPad Prism 8 (GraphPad Software, Inc., La Jolla, CA, USA). Comparisons between two groups were conducted by the method of *t*-test. Comparisons among three or more group were done using one-way ANOVA. $P<0.05$ was considered as statistically significant.

Acknowledgements

We thank Miss Zhangyufan He from Huashan Hospital, Fudan University, for her kind help with the language polishing. This work was funded by the National Natural Science Foundation of China (Grant No. 81971559, 82041010, 81971900, 31872744), National Science and Technology Major Project (Grant No. 2018ZX10731301-004, 2018ZX10302302-002 and 2018ZX10301-404-002-003) and the Science and Technology Commission of Shanghai Municipality (Grant No. 20411950400).

Author contributions

Y.M.W., Y.X., C.Q., Z.Q.Z. and W.H.Z. designed the study. L.Q.J., S.F.W., Y.M.W., X.X.T., Y.F.Z., J.W., X.Y.W., and J.W. conducted the experiments. Y.M.W., L.Q.J. and S.F.W. analyzed the data and drafted the manuscript. Y.M.W., Y.X., C.Q., Z.Q.Z. and W.H.Z. revised the manuscript. D.M.Y. and W.H.W. provided intellectual inputs in tackling technical challenges in tracking the potential cross-reacting antigens.

Conflict of Interest

The authors declare that they have no relevant conflicts of interest.

Data availability

The data of metagenomic analysis of gut microbiota has been deposited to the

694 NCBI Sequence Read Archive (SRA) database with the accession number
695 PRJNA747837.

696

697 ## References

698 1. Lu LL, Suscovich TJ, Fortune SM, Alter G. Beyond binding: antibody effector functions in
699 infectious diseases. Nature reviews Immunology. 2018;18(1):46-61.
700 2. Warter L, Appanna R, Fink K. Human poly- and cross-reactive anti-viral antibodies and their
701 impact on protection and pathology. Immunologic research. 2012;53(1-3):148-61.
702 3. Cobey S, Hensley SE. Immune history and influenza virus susceptibility. Current opinion in
703 virology. 2017;22:105-11.
704 4. Mok DZL, Chan KR. The Effects of Pre-Existing Antibodies on Live-Attenuated Viral Vaccines.
705 Viruses. 2020;12(5).
706 5. Zimmermann P, Curtis N. Factors That Influence the Immune Response to Vaccination. Clinical
707 microbiology reviews. 2019;32(2).
708 6. Dugan HL, Guthmiller JJ, Arevalo P, Huang M, Chen YQ, Neu KE, et al. Preexisting immunity
709 shapes distinct antibody landscapes after influenza virus infection and vaccination in humans. Science
710 translational medicine. 2020;12(573).
711 7. Zhang A, Stacey HD, Mullarkey CE, Miller MS. Original Antigenic Sin: How First Exposure
712 Shapes Lifelong Anti-Influenza Virus Immune Responses. Journal of immunology (Baltimore, Md :
713 1950). 2019;202(2):335-40.
714 8. Boes M. Role of natural and immune IgM antibodies in immune responses. Molecular
715 immunology. 2000;37(18):1141-9.
716 9. Auladell M, Jia X, Hensen L, Chua B, Fox A, Nguyen THO, et al. Recalling the Future:
717 Immunological Memory Toward Unpredictable Influenza Viruses. Frontiers in immunology.
718 2019;10:1400.
719 10. St. John AL, Rathore APS. Adaptive immune responses to primary and secondary dengue virus
720 infections. Nature Reviews Immunology. 2019;19(4):218-30.
721 11. Izmirly AM, Alturki SO, Alturki SO, Connors J, Haddad EK. Challenges in Dengue Vaccines
722 Development: Pre-existing Infections and Cross-Reactivity. 2020;11(1055).
723 12. Andrade P, Gimblet-Ochieng C, Modirian F, Collins M, Cárdenas M, Katzelnick LC, et al. Impact
724 of pre-existing dengue immunity on human antibody and memory B cell responses to Zika. Nature
725 Communications. 2019;10(1):938.
726 13. Liao HX, Chen X, Munshaw S, Zhang R, Marshall DJ, Vandergrift N, et al. Initial antibodies
727 binding to HIV-1 gp41 in acutely infected subjects are polyreactive and highly mutated. The Journal of
728 experimental medicine. 2011;208(11):2237-49.
729 14. Bonsignori M, Liao HX, Gao F, Williams WB, Alam SM, Montefiori DC, et al. Antibody-virus
730 co-evolution in HIV infection: paths for HIV vaccine development. Immunological reviews.
731 2017;275(1):145-60.
732 15. Williams WB, Liao HX, Moody MA, Kepler TB, Alam SM, Gao F, et al. HIV-1 VACCINES.
733 Diversion of HIV-1 vaccine-induced immunity by gp41-microbiota cross-reactive antibodies. Science
734 (New York, NY). 2015;349(6249):aab1253.
735 16. Zitvogel L, Ayyoub M, Routy B, Kroemer G. Microbiome and Anticancer Immunosurveillance.
736 Cell. 2016;165(2):276-87.

17. Leng Q, Tarbe M, Long Q, Wang F. Pre-existing heterologous T-cell immunity and neoantigen immunogenicity. Clinical & translational immunology. 2020;9(3):e01111.
18. Sioud M. T-cell cross-reactivity may explain the large variation in how cancer patients respond to checkpoint inhibitors. Scandinavian journal of immunology. 2018;87(3).
19. Rose NR. Negative selection, epitope mimicry and autoimmunity. Current opinion in immunology. 2017;49:51-5.
20. Anderson EM, Goodwin EC, Verma A, Arevalo CP, Bolton MJ, Weirick ME, et al. Seasonal human coronavirus antibodies are boosted upon SARS-CoV-2 infection but not associated with protection. Cell. 2021.
21. Galipeau Y, Greig M, Liu G, Driedger M, Langlois MA. Humoral Responses and Serological Assays in SARS-CoV-2 Infections. Frontiers in immunology. 2020;11:610688.
22. Klompus S, Leviatan S, Vogl T, Kalka IN, Godneva A, Shinar E, et al. Cross-reactive antibody responses against SARS-CoV-2 and seasonal common cold coronaviruses. 2020:2020.09.01.20182220.
23. Shrock E, Fujimura E, Kula T, Timms RT, Lee IH, Leng Y, et al. Viral epitope profiling of COVID-19 patients reveals cross-reactivity and correlates of severity. Science (New York, NY). 2020;370(6520).
24. Ortega N, Ribes M, Vidal M, Rubio R, Aguilar R, Williams S, et al. Seven-month kinetics of SARS-CoV-2 antibodies and protective role of pre-existing antibodies to seasonal human coronaviruses on COVID-19. 2021:2021.02.22.21252150.
25. Ladner JT, Henson SN, Boyle AS, Engelbrektson AL, Fink ZW, Rahee F, et al. Epitope-resolved profiling of the SARS-CoV-2 antibody response identifies cross-reactivity with endemic human coronaviruses. Cell reports Medicine. 2021;2(1):100189.
26. Ng KW, Faulkner N, Cornish GH, Rosa A, Harvey R, Hussain S, et al. Preexisting and de novo humoral immunity to SARS-CoV-2 in humans. Science (New York, NY). 2020;370(6522):1339-43.
27. Yang R, Lan J, Huang B, A R, Lu M, Wang W, et al. Lack of antibody-mediated cross-protection between SARS-CoV-2 and SARS-CoV infections. EBioMedicine. 2020;58:102890.
28. Lv H, Wu NC, Tsang OT, Yuan M, Perera R, Leung WS, et al. Cross-reactive Antibody Response between SARS-CoV-2 and SARS-CoV Infections. Cell reports. 2020;31(9):107725.
29. Zhu Y, Yu D, Han Y, Yan H, Chong H, Ren L, et al. Cross-reactive neutralization of SARS-CoV-2 by serum antibodies from recovered SARS patients and immunized animals. Science advances. 2020;6(45).
30. Lipsitch M, Grad YH, Sette A, Crotty S. Cross-reactive memory T cells and herd immunity to SARS-CoV-2. Nature reviews Immunology. 2020;20(11):709-13.
31. Sumbul B, Sumbul HE, Okyay RA, Gülümsek E, Şahin AR, Boral B, et al. Is there a link between pre-existing antibodies acquired due to childhood vaccinations or past infections and COVID-19? A case control study. PeerJ. 2021;9:e10910.
32. Majdoubi A, Michalski C, O'Connell SE, Dada S, Narpala SR, Gelinas JP, et al. A majority of uninfected adults show pre-existing antibody reactivity against SARS-CoV-2. JCI insight. 2021.
33. Sette A, Crotty S. Pre-existing immunity to SARS-CoV-2: the knowns and unknowns. Nature reviews Immunology. 2020;20(8):457-8.
34. Tso FY, Lidenge SJ, Peña PB, Clegg AA, Ngowi JR, Mwaiselage J, et al. High prevalence of pre-existing serological cross-reactivity against severe acute respiratory syndrome coronavirus-2 (SARS-CoV-2) in sub-Saharan Africa. International journal of infectious diseases : IJID : official publication of the International Society for Infectious Diseases. 2021;102:577-83.

781 35. Lee CH, Pinho MP, Buckley PR, Woodhouse IB, Ogg G, Simmons A, et al. Potential CD8+ T Cell
782 Cross-Reactivity Against SARS-CoV-2 Conferred by Other Coronavirus Strains. Frontiers in
783 immunology. 2020;11:579480.
784 36. Freeman B, Lester S, Mills L, Rasheed MAU, Moye S, Abiona O, et al. Validation of a
785 SARS-CoV-2 spike protein ELISA for use in contact investigations and sero-surveillance.
786 2020:2020.04.24.057323.
787 37. Post N, Eddy D, Huntley C, van Schalkwyk MCI, Shrotri M, Leeman D, et al. Antibody response
788 to SARS-CoV-2 infection in humans: A systematic review. PloS one. 2020;15(12):e0244126.
789 38. Reche PA. Potential Cross-Reactive Immunity to SARS-CoV-2 From Common Human Pathogens
790 and Vaccines. Frontiers in immunology. 2020;11:586984.
791 39. Doshi P. Covid-19: Do many people have pre-existing immunity? 2020;370:m3563.
792 40. Steiner S, Sotzny F, Bauer S, Na I-K, Schmueck-Henneresse M, Corman VM, et al. HCoV- and
793 SARS-CoV-2 Cross-Reactive T Cells in CVID Patients. 2020;11(3347).
794 41. Mateus J, Grifoni A, Tarke A, Sidney J, Ramirez SI, Dan JM, et al. Selective and cross-reactive
795 SARS-CoV-2 T cell epitopes in unexposed humans. 2020;370(6512):89-94.
796 42. Grifoni A, Weiskopf D, Ramirez SI, Mateus J, Dan JM, Moderbacher CR, et al. Targets of T Cell
797 Responses to SARS-CoV-2 Coronavirus in Humans with COVID-19 Disease and Unexposed
798 Individuals. Cell. 2020;181(7):1489-501.e15.
799 43. Braun J, Loyal L, Frentsch M, Wendisch D, Georg P, Kurth F, et al. SARS-CoV-2-reactive T cells
800 in healthy donors and patients with COVID-19. Nature. 2020;587(7833):270-4.
801 44. Kim H, Seiler P, Jones JC, Ridout G, Camp KP, Fabrizio TP, et al. Antibody Responses to
802 SARS-CoV-2 Antigens in Humans and Animals. Vaccines. 2020;8(4).
803 45. Anderson EM, Goodwin EC, Verma A, Arevalo CP, Bolton MJ, Weirick ME, et al. Seasonal
804 human coronavirus antibodies are boosted upon SARS-CoV-2 infection but not associated with
805 protection. Cell. 2021;184(7):1858-64.e10.
806 46. Song G, He W-t, Callaghan S, Anzanello F, Huang D, Ricketts J, et al. Cross-reactive serum and
807 memory B-cell responses to spike protein in SARS-CoV-2 and endemic coronavirus infection. Nature
808 Communications. 2021;12(1):2938.
809 47. Fraley E, LeMaster C, Banerjee D, Khanal S, Selvarangan R, Bradley T. Cross-reactive antibody
810 immunity against SARS-CoV-2 in children and adults. Cellular & molecular immunology. 2021:1-3.
811 48. Nguyen-Contant P, Embong AK, Kanagaiah P, Chaves FA, Yang H, Branche AR, et al. S
812 Protein-Reactive IgG and Memory B Cell Production after Human SARS-CoV-2 Infection Includes
813 Broad Reactivity to the S2 Subunit. mBio. 2020;11(5).
814 49. Zhao Q, Elson CO. Adaptive immune education by gut microbiota antigens. Immunology.
815 2018;154(1):28-37.
816 50. Bradt V, Malafa S, von Braun A, Jarmer J, Tsouchnikas G, Medits I, et al. Pre-existing yellow
817 fever immunity impairs and modulates the antibody response to tick-borne encephalitis vaccination.
818 NPJ vaccines. 2019;4:38.
819 51. Pinto D, Sauer MM, Czudnochowski N, Low JS, Tortorici MA, Housley MP, et al. Broad
820 betacoronavirus neutralization by a stem helix-specific human antibody. Science (New York, NY).
821 2021.
822 52. Lee IC, Huo TI, Huang YH. Gastrointestinal and liver manifestations in patients with COVID-19.
823 Journal of the Chinese Medical Association : JCMA. 2020;83(6):521-3.
824 53. Jin X, Lian JS, Hu JH, Gao J, Zheng L, Zhang YM, et al. Epidemiological, clinical and virological

characteristics of 74 cases of coronavirus-infected disease 2019 (COVID-19) with gastrointestinal symptoms. Gut. 2020;69(6):1002-9.

54. Mao R, Qiu Y, He JS, Tan JY, Li XH, Liang J, et al. Manifestations and prognosis of gastrointestinal and liver involvement in patients with COVID-19: a systematic review and meta-analysis. The lancet Gastroenterology & hepatology. 2020;5(7):667-78.

55. Fan W, Wan Y, Li Q. Interleukin-21 enhances the antibody avidity elicited by DNA prime and MVA boost vaccine. Cytokine. 2020;125:154814.

56. Lu S, Manning S, Arthos J. Antigen engineering in DNA immunization. Methods in molecular medicine. 2000;29:355-74.

57. Nie J, Li Q, Wu J, Zhao C, Hao H, Liu H, et al. Establishment and validation of a pseudovirus neutralization assay for SARS-CoV-2. Emerging microbes & infections. 2020;9(1):680-6.

58. Li Q, Wu J, Nie J, Zhang L, Hao H, Liu S, et al. The Impact of Mutations in SARS-CoV-2 Spike on Viral Infectivity and Antigenicity. Cell. 2020;182(5):1284-94.e9.

59. Ren Y, Wang N, Hu W, Zhang X, Xu J, Wan Y. Successive site translocating inoculation potentiates DNA/recombinant vaccinia vaccination. Scientific reports. 2015;5:18099.

Figure legends

Figure 1. Pre-existing cross-reactive antibodies against SARS-CoV-2 S protein observed in both healthy human and naïve SPF mice predominantly targeted S2

The pre-existing cross-reactive antibodies against S1 and S2 were measured using an in-house ELISA (Sample dilution factor: 100). (**A**) Plasma samples of healthy individuals collected in 2020 (n=95). (**B**) Plasma samples of healthy individuals collected in 2016 (n=78). (**C**) Sera of naïve C56BL/6J mice (n=12). (**D**) Sera of naïve BALB/c mice (n=101). The dot lines showed the threshold of background (3 folds of the background OD). Statistical analyses were performed using the method of paired t-test.

Figure 2 The pre-existing S protein binding antibodies in naïve SPF mice recognized S2 exclusively and a dominant linear antibody epitope was identified on the connector domain

The pre-existing S1 and S2 cross-reactive antibody levels of 6 mice selected for WB assays were shown in (**A**). (**B**) Western-blotting assays of pre-existing cross-reactive antibodies for 6 selected mouse serum samples. The purities of S1 and S2 proteins were shown by coomassie blue staining. (**C**) The minimal epitope of P144 was defined using a method of competitive ELISA (Data shown as mean±SD, n=5). Purified S2 protein was used as the coating antigen and truncated peptides derived from P144 were used as competitors. The decreases of competitive inhibition reflected the necessity of each amino acid for the epitope recognition. Statistical differences among groups was analyzed using One-way ANOVA. ****, P<0.0001. M: molecular weight markers; SP, signal peptide; RBD, receptor-binding domain; FP, fusion peptide; HR, heptad repeat; CH, central helix; CD, connector domain; TM, transmembrane domain; CT, cytoplasmic tail.

Figure 3 Cross-reactive antibodies recognizing epitope P144 widely existed in both healthy human and naïve SPF mice

P144 specific binding antibodies were detected using a method of competitive ELISA. (**A**) For the detections of P144 specific binding antibodies in naïve SPF mice, purified S2 protein was used as the coating antigen and P144 peptide

was used as the competitor. (**B**) For the detections of P144 specific binding antibodies in healthy individuals, purified BSA-P144 conjugate was used as the coating antigen and P144 peptide was used as the competitor. In both experiments, the reduction of OD value reflected the presence of P144 binding antibodies.

Figure 4 The generation of the pre-existing S2 cross-reactive antibodies were associated with commensal gut microbiota

(**A**) Comparison of the levels of S2 specific pre-existing antibodies between naïve mice maintained under SPF condition and mice in a sterile isolation pack. (**B**) Comparison of commensal gut bacteria compositions between mice housed in a SPF facility and mice in a sterile isolation pack by metagenomic sequencing. Differences of bacterial abundance was analyzed by linear discriminant analysis (LDA) analysis and shown as the histogram of LDA scores. It was considered a significant effect size with LDA score > 4.0. (p), Phylum. (c), Class. (o), Order. (f), Family. (g), Genus. (s), Species. **(C)** Schematic overview of the fecal bacteria transplantation (n=6). The mice bred in the isolation pack were treated with a mixture of ampicillin (1g/L), metronidazole (0.5g/L), vancomycin (0.5g/L) and gentamycin (0.5g/L) dissovled in drinking water supplemented with D-glucose (36.8g/L) for 14 days. Two weeks after antibiotic treatment, fecal bacteria were freshly prepared from SPF mice and delivered via oral gavage. **(D)** P144 specific antibody was determined using an in-house ELISA method. Data are shown as mean±SD (n=6). Statistical analyses were performed by the method of paired t-test.

Figure 5 P144 specific monoclonal antibodies isolated from naïve SPF mice cross-reacted with commensal gut bacteria from both human and mouse

Cross-reactivities between P144 specific mAbs and gut microbial antigens were detected using WB assays. A purified mouse IgG was used as the control. (**A**) WB assays of mouse fecal bacteria samples. L: mixed fecal bacteria samples collected from 3 mice with low levels of pre-existing S2 binding antibodies ($OD_{450nm-630nm} \leqslant 0.140$ at serum dilution of 1:100); H: mixed fecal bacteria samples collected from 3 mice with high levels of pre-existing S2

binding antibodies ($OD_{450nm-630nm} \geqslant 0.615$ at serum dilution of 1:100). (**B**) WB assays of fecal bacteria samples collected from 7 healthy individuals (Lanes 1-7). All the mAbs and the control mouse IgG were diluted at the final concentration of 1μg/ml. Black arrows indicated the locations of protein bands chosen for the Mass spectrometry analysis.

Figure 6 Impact of pre-existing antibodies on the humoral immune responses elicited by a DNA vaccine encoding SARS-CoV-2 S protein

(**A**) Schematic illustration of the vaccination regimen. 50μg of the candidate DNA vaccine was injected intra muscularly into each mice at week 0, week 2 and week 4. Two weeks after the final vaccination, the mice was sacrificed for the measurements of specific immune responses. (**B**) Periphral blood was collected before immunization and levels of pre-existing S2 specific IgG were compared among three groups of mice. (**C**) Comparisons of endpoint IgG titers against S2 in the serum of mice measured at 2 weeks post the last immunization. (**D**) Comparisons of P144 specific IgG titers in the serum of mice as measured using BSA-P144 conjugate as the coating antigen. (**E**) Comparisons of P144 specific binding antibody levels as determined using a method of competitive ELISA. (**F**) Endpoint IgG titers against S1 measured at 2 weeks post the final vaccination. (**G**) Neutralizing antibody titers against SARS-CoV-2 D614G pseudo-virus in serum of mice at 2 weeks post the final immunization. The vaccination experiment was repeated twice with 6 mice for each group. Data were shown as mean±SD. Statistical analyses were performed by the method of one-way ANONVA.

Figure 7 The impact of pre-existing antibody on the levels of specific IgG and IgA in BALF after vaccination

BALF was collected from each mouse after euthanasia. Specific IgG (A and B) and IgA (C and D) against S1 or S2 were detected using in-house ELISA methods. All the BALF samples were adjusted to the initial total protein concentration of 51.9μg/ml. Data are shown as mean± SD. Statistical analyses were performed by the method of one-way ANONVA.

Figure 8 The impact of pre-existing antibody on the minimum epitope recognition of P144 after vaccination.

The minimal epitope recognized by mouse sera after vaccination were analyzed using a method of competitive ELISA. Purified BSA-P144 conjugate was used as the coating antigen and truncated peptides derived from P144 were used as the competitors. The decreases of competitive inhibition reflected the necessity of each amino acid for the epitope recognition. Statistical analyses were performed by the method of two-tailed t-test (*, $P< 0.05$, **, $P< 0.01$, ***, $P< 0.001$).

Figure 9 The impact of pre-existing antibody on the cellular immune responses after vaccination

(**A**) The diagram of the method for cellular immune responses assays. (**B**) S1 and S2 specific IFN-γ responses were compared among groups of mice with different levels of pre-existing S2 cross-reactive antibodies. Additionally, S1 (**C**) and S2 (**D**) specific releases of IL-2, IL-6 and TNF-α as measured using the method of multiplex cytokine bead assay were also compared among different groups. Data were shown as mean$\pm$ SD. SFU, spot forming units.

Figure 10 Levels of pre-existing S2 cross-reactive antibody correlated with RBD binding antibody responses elicited by an inactivated SARS-CoV-2 vaccine

(A) Peripheral blood samples were collected from 28 healthy vaccinees who received two doses of an inactivated SARS-CoV-2 vaccine at baseline and 14 days post 2nd dose, respectively. The RBD binding antibody titers were measured by ELISA. The neutralizing antibody responses were quantified by a commercialized surrogate virus neutralization test (sVNT) (Suzhou Sym-Bio Life Science Co., Ltd). **(B and C**) Correlations between RBD binding antibody titers and levels of pre-existing S2 or P144 specific IgG. **(D)** Correlation between neutralizing antibody concentrations and pre-existing P144 binding antibody levels. Statistical analyses were performed using the method of Spearman's correlation**.**

Supplementary figures

Supplementary Figure 1 A dominant linear epitope recognized by the pre-existing antibodies was located on the connector domain of S2

(**A**) The location of P144 on the full length of SARS-CoV-2 spike protein. Synthesized peptides (18-mer, overlapped by 11amino acids) spanning the full length of S2 were divided into 9 peptide pools, each contained 8 peptides. To identify the potential antibody binding epitopes, we first performed competitive ELISA assays using the peptide pools as competitors (Data not shown). The pool showing significant inhibition effect was further delineated by testing the inhibiting efficiencies of each individual peptides (**B**).The data was shown as mean±SD, n=5. Inhibition efficiencies among groups were analyzed using the method of One-way ANOVA. ****, $p<0.0001$. SP, signal peptide; RBD, receptor-binding domain; FP, fusion peptide; HR, heptad repeat; CH, central helix; CD, connector domain; TM, transmembrane domain; CT, cytoplasmic tail.

Supplementary Figure 2 Phylogenetic analysis of the spike protein sequences of major human coronaviruses

The sequences of SARS-CoV-2 Wuhan (YP_009724390), MERS-CoV (QFQ59587.1), HCoV-OC43 (QDH43719.1), HCoV-NL63 (AKT07952), HCoV-229E (AOG74783.1) and HCoV-HKU1 (YP_173238) were retrieved from NCBI database. The sequences of B.1.1.7, D614G, B.1.351, B.1.525, B.1.617 and P.1(B.1.1.281) were obtained from Global Initiative on Sharing Avian Influenza Data (GISAID). Boxed fragments represent IEDB predicted linear antibody epitope (http://tools.iedb.org/bcell/).

Supplementary Figure 3 Evidences that implied the link between pre-existing S2 cross-reactive antibodies and commensal gut bacteria

(**A**) Principle component analysis (PCA) of gut microbial communities between 4 mice in SPF condition and 4 mice in a sterile isolation pack. (**B**) The splenocytes and lymphocytes of MLN were harvested from 4 naive C57BL/6J mice with relatively high levels of pre-existing S2 cross-reactive antibodies. S2 specific B cells were defined as $CD45^{+}CD19^{+}S2^{+}$ (Left). Statistical analysis was performed by the method of paired t-test (Right).

Supplementary Figure 4 Characterizations of the minimal epitope recognitions for the 6 monoclonal antibodies isolated from naïve mice

Six P144 specific monoclonal antibodies were isolated from 2 naïve SPF mice using the hybridoma technology. (**A**) The minimum epitope recognitions of clones H9, E10, G13, F5 and G18 were similar detected by a method of competitive ELISA. Purified S2 protein was used as the coating antigen and the truncated peptides derived from P144 were used as the competitors. (**B**) The epitope recognition of clone M3 was analyzed using purified S2 protein as the coating antigen and each listed peptide was used as the competitor. SP, signal peptide; RBD, receptor-binding domain; FP, fusion peptide; HR, heptad repeat; CH, central helix; CD, connector domain; TM, transmembrane domain; CT, cytoplasmic tail.

Supplementary Figure 5 Neutralizing activities of the purified monoclonal antibodies as measured using a pseudo virus neutralization assay

Neutralization activities of 6 isolated mAbs against 5 major SARS-CoV-2 variants (D614G, B.1.617, B.1.1.7, B.1.351 and P.1) were examined using a pseudo virus neutralization assay. Purified mouse IgG was used as negative control and serum of an RBD protein vaccinated goat was use as positive control. Purified mAbs and control mouse IgG were tested at a concentration of 1μg/ml; positive goat serum was diluted at 1:90.

Supplementary Figure 6 Validation of cross-reactivity between P144 specific mAb and *E. coli*

Proteins in the WCL of *E. coli* (strain DH5α) were separated by SDS-PAGE. The cross-reactivity between *E. coli* and P144 specific mAb (clone F5) was determined by western blotting. F5 or a purified mouse IgG was used as the first antibody at the concentration of 1 μg/ml. Black arrows pointed out the bands with MWs equal to *E. coli* proteins identified by LCMS analysis.

Figures and Figure legends

Figure 1

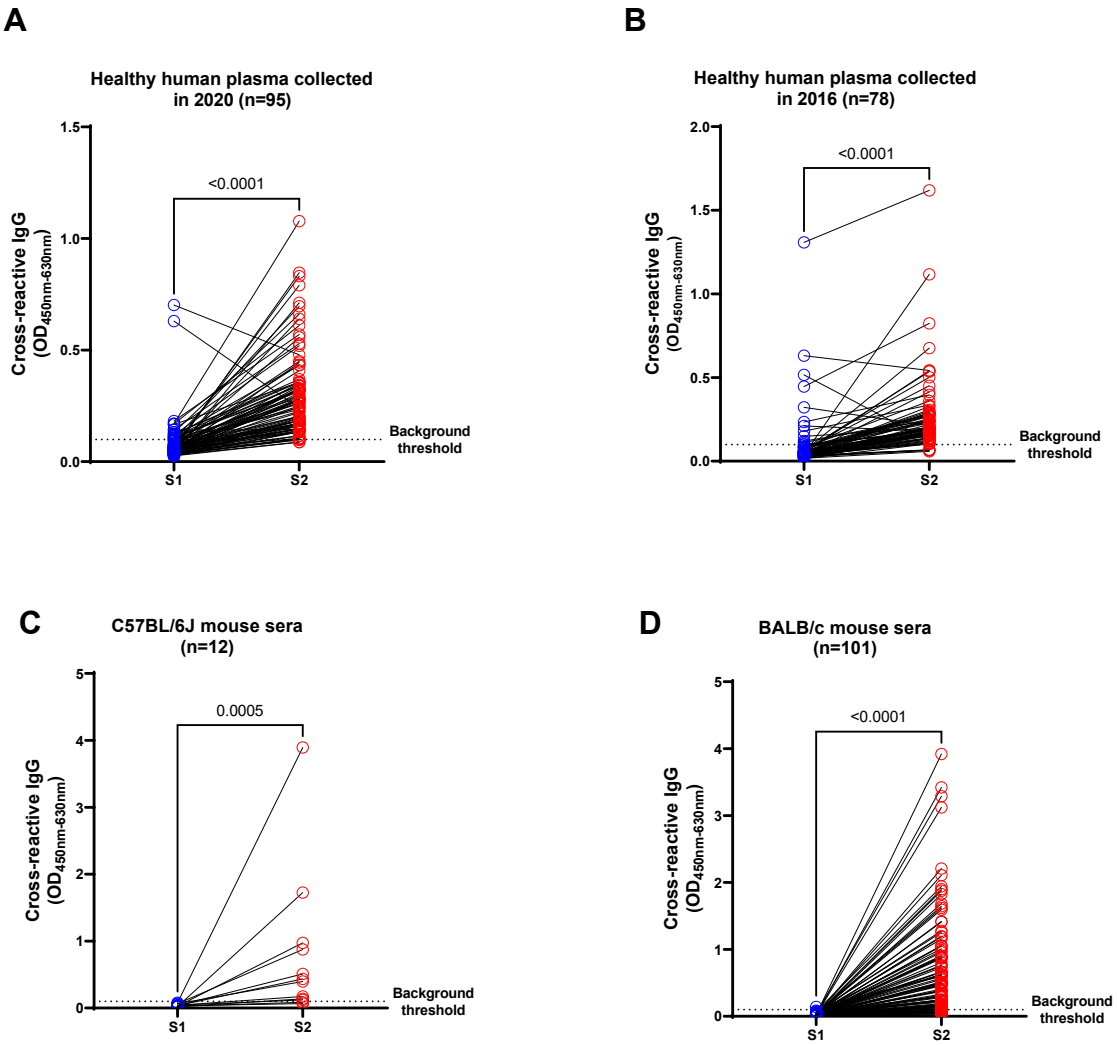

Figure 1. Pre-existing cross-reactive antibodies against SARS-CoV-2 S protein observed in both healthy human and naïve SPF mice predominantly targeted S2 subunit. The pre-existing cross-reactive antibodies against S1 and S2 were measured using an in-house ELISA (Sample dilution factor: 100). (**A**) Plasma samples of healthy individuals collected in 2020 (n=95). (**B**) Plasma samples of healthy individuals collected in 2016 (n=78). (**C**) Sera of naïve C57BL/6J mice (n=12). (**D**) Sera of naïve BALB/c mice (n=101). The dot lines showed the threshold of background (3 folds of the background OD). Statistical analyses were performed using the method of paired t-test.

Figure 2

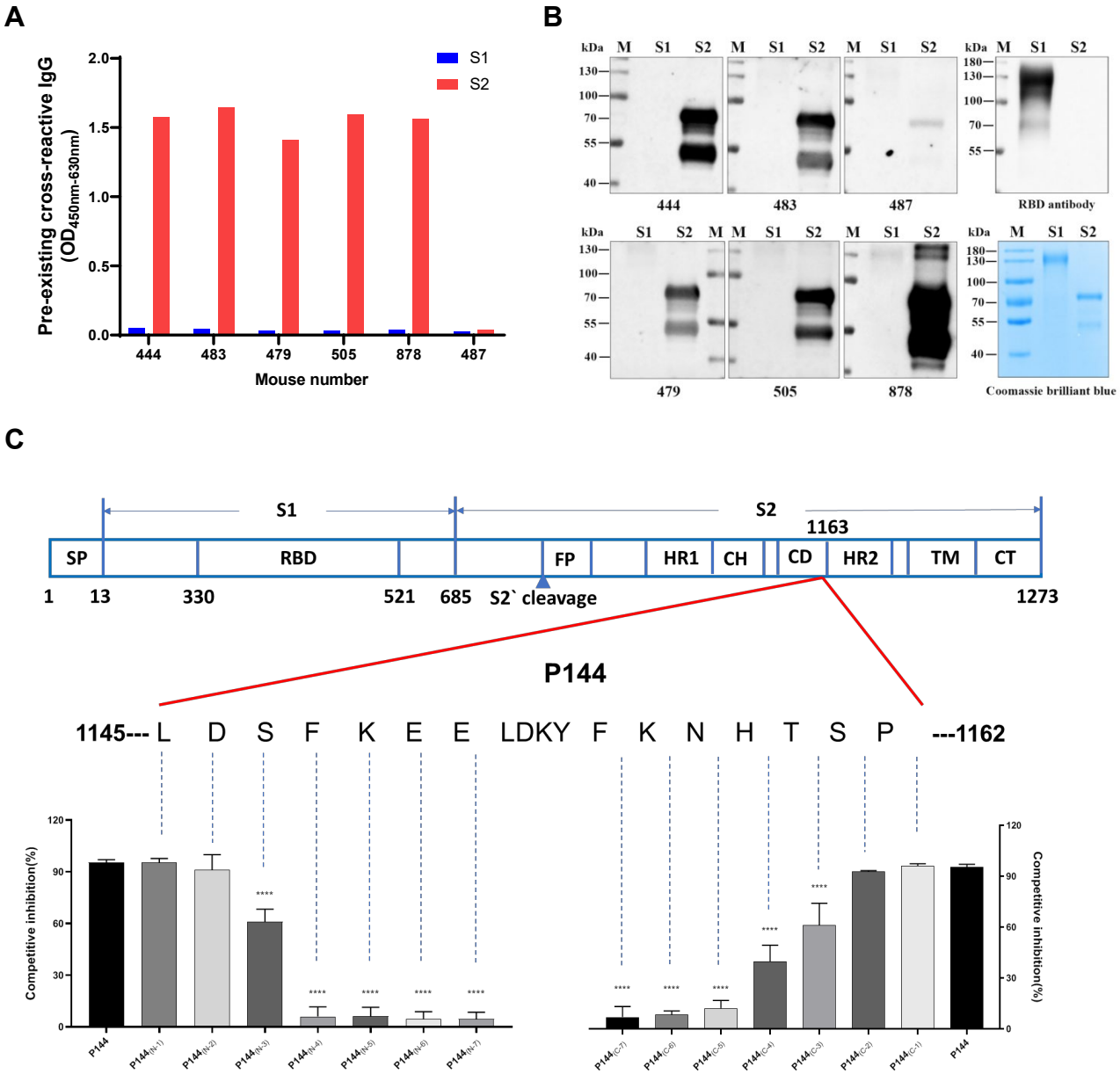

Figure 2. The pre-existing S protein binding antibodies in naïve SPF mice recognized S2 exclusively and a dominant linear antibody epitope was identified on the connector domain. The pre-existing S1 and S2 cross-reactive antibody levels of 6 mice selected for WB assays were shown in (**A**). (**B**) Western-blotting assays of pre-existing cross-reactive antibodies for 6 selected mouse serum samples. The purities of S1 and S2 proteins were shown by coomassie blue staining. (**C**) The minimal epitope of P144 was defined using a method of competitive ELISA (Data shown as mean±SD, n=5). Purified S2 protein was used as the coating antigen and truncated peptides derived from P144 were used as competitors. The decreases of competitive inhibition reflected the necessity of each amino acid for the epitope recognition. Statistical differences among groups was analyzed using One-way ANOVA. ****, P<0.0001. M: molecular weight markers; SP, signal peptide; RBD, receptor-binding domain; FP, fusion peptide; HR, heptad repeat; CH, central helix; CD, connector domain; TM, transmembrane domain; CT, cytoplasmic tail.

Figure 3

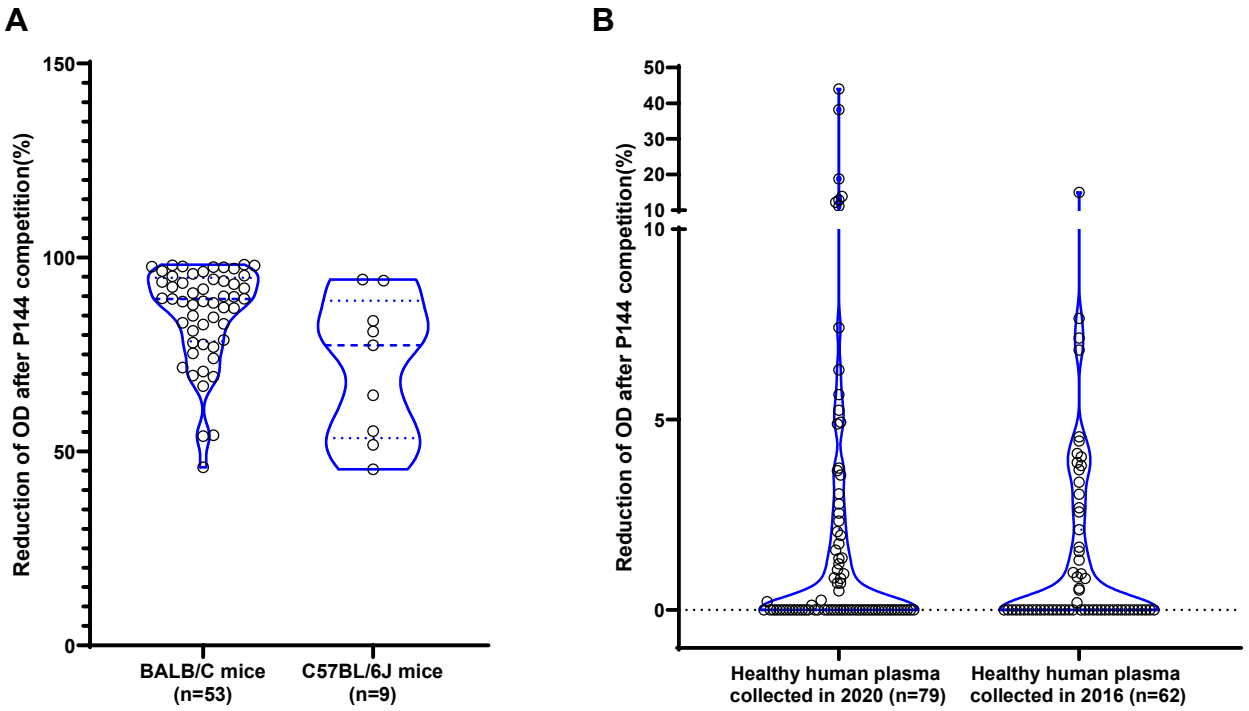

Figure 3. Cross-reactive antibodies recognizing epitope P144 widely existed in both healthy human and naïve SPF mice. P144 specific binding antibodies were detected using a method of competitive ELISA. (**A**) For the detections of P144 specific binding antibodies in naïve SPF mice, purified S2 protein was used as the coating antigen and P144 peptide was used as the competitor. (**B**) For the detections of P144 specific binding antibodies in healthy individuals, purified BSA-P144 conjugate was used as the coating antigen and P144 peptide was used as the competitor. In both experiments, the reduction of OD value reflected the presence of P144 binding antibodies.

Figure 4

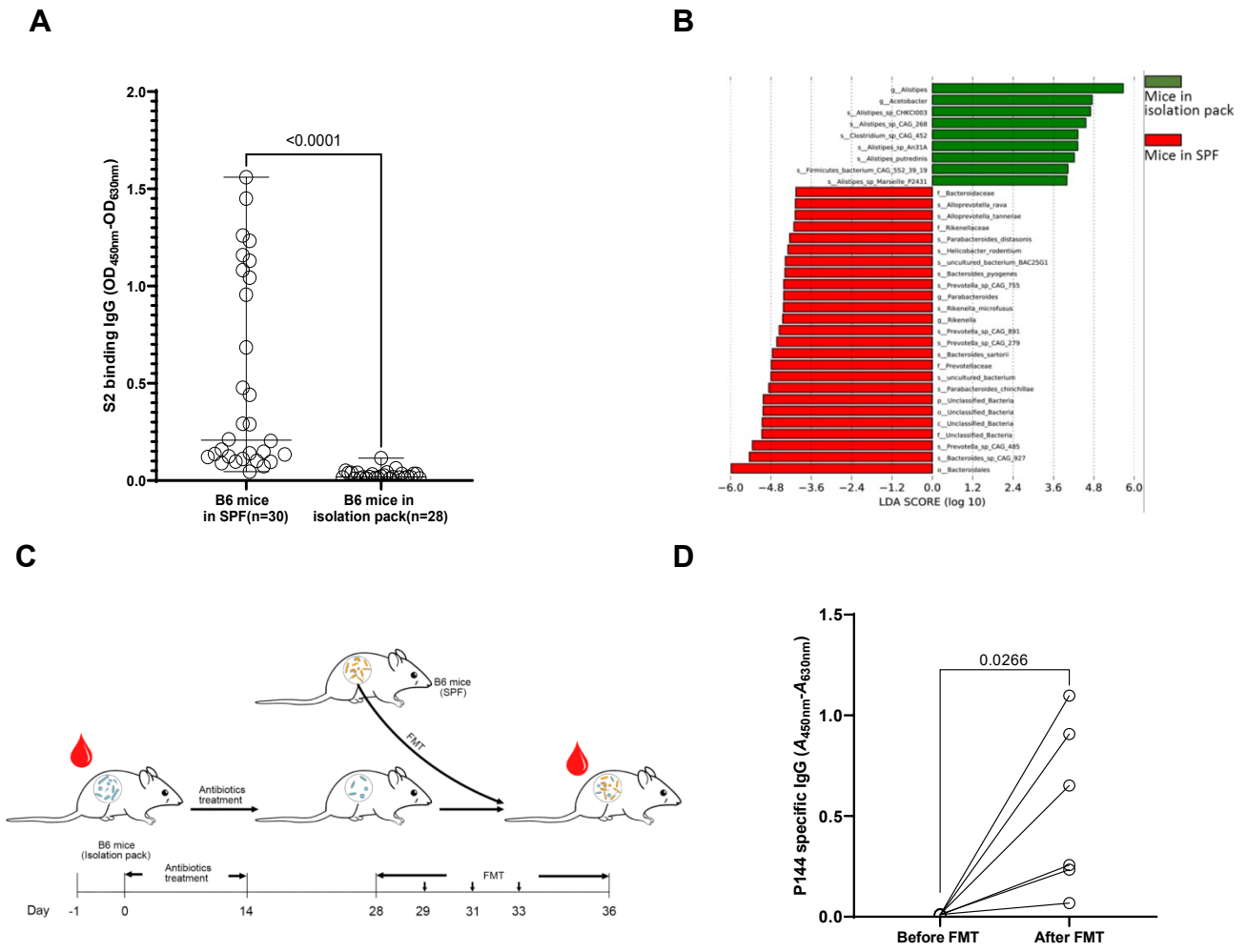

Figure 4. The generation of the pre-existing S2 cross-reactive antibodies might be associated with commensal gut microbiota. (**A**) Comparison of the levels of S2 specific pre-existing antibodies between naïve mice maintained under SPF condition and mice in a sterile isolation pack. (**B**) Comparison of commensal gut bacteria compositions between mice housed in a SPF facility and mice in a sterile isolation pack by metagenomic sequencing. Differences of bacterial abundance was analyzed by linear discriminant analysis (LDA) analysis and shown as the histogram of LDA scores. It was considered a significant effect size with LDA score > 4.0. (p), Phylum. (c), Class. (o), Order. (f), Family. (g), Genus. (s), Species. **(C and D)** P144 specific antibodies were induced in mice bred in the isolation pack after being transplanted with fecal bacteria isolated from SPF mice. **(C)** Schematic overview of the fecal bacteria transplantation (n=6). The mice bred in the isolation pack were treated with a mixture of ampicillin (1g/L), metronidazole (0.5g/L), vancomycin (0.5g/L) and gentamycin (0.5g/L) in drinking water supplemented with D-glucose (36.8g/L) for 14 days. Two weeks after antibiotic treatment, fecal bacteria were freshly prepared from SPF mice and delivered via oral gavage. **(D)** For the detections of P144 cross-reactive antibodies, purified BSA-P144 conjugate was used as the coating antigen and specific binding antibody was determined using an in-house ELISA method. Data are shown as mean±SD. Statistical analyses were performed by the method of paired t-test.

Figure 5

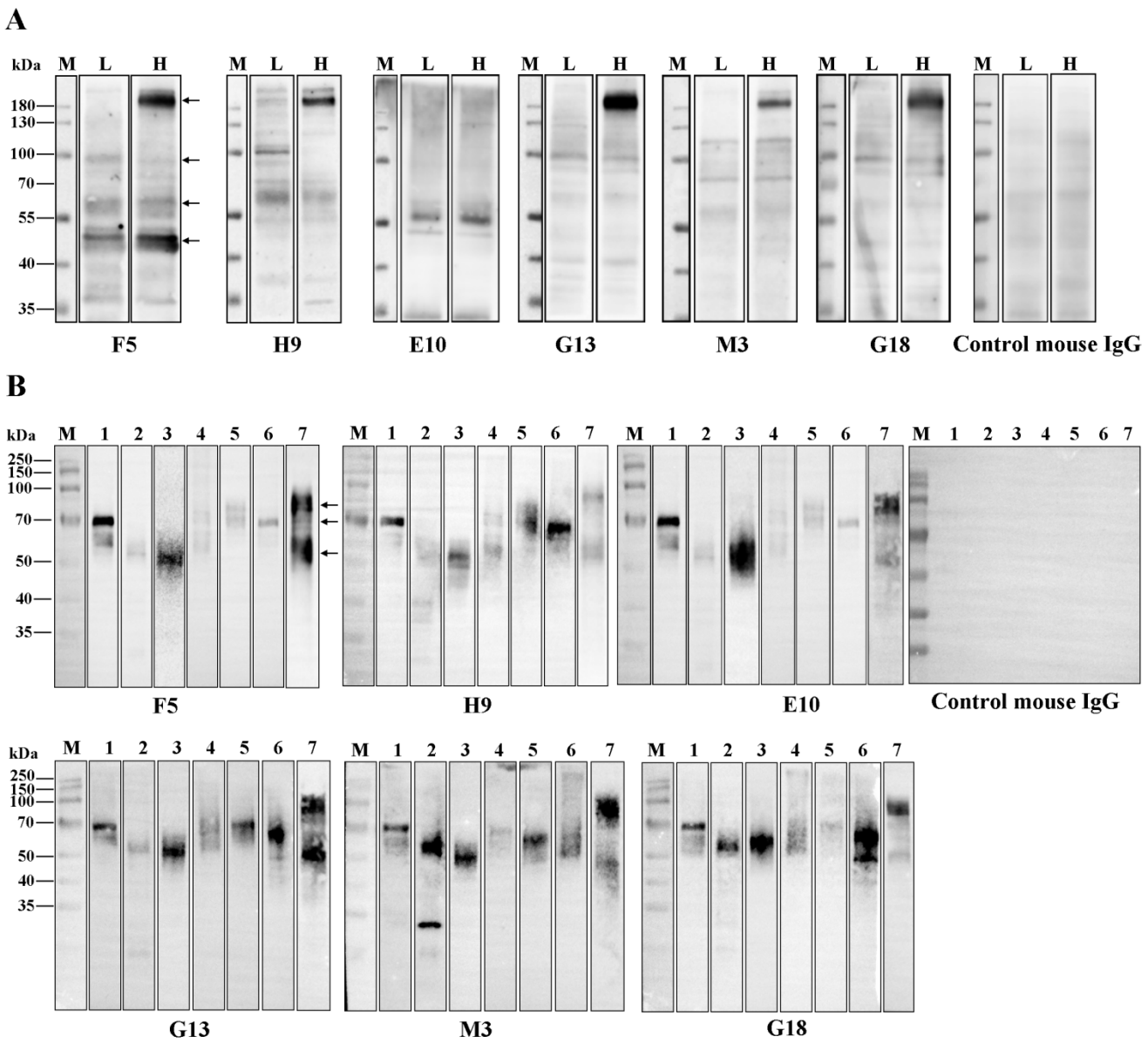

Figure 5. P144 specific monoclonal antibodies isolated from naïve SPF mice cross-reacted with commensal gut bacteria from both human and mouse. Cross-reactivities between P144 specific mAbs and gut microbial antigens were detected using WB assays. A purified mouse IgG was used as the control. (**A**) WB assays of mouse fecal bacteria samples. L: mixed fecal bacteria samples collected from 3 mice with low levels of pre-existing S2 binding antibodies ($OD_{450nm-630nm}$≤0.140 at serum dilution of 1:100); H: mixed fecal bacteria samples collected from 3 mice with high levels of pre-existing S2 binding antibodies ($OD_{450nm-630nm}$≥0.615 at serum dilution of 1:100). (**B**) WB assays of fecal bacteria samples collected from 7 healthy individuals (Lanes 1-7). All the mAbs and the control mouse IgG were diluted at the final concentration of 1μg/ml. Black arrows indicated the locations of protein bands chosen for the Mass spectrometry analysis.

Figure 6

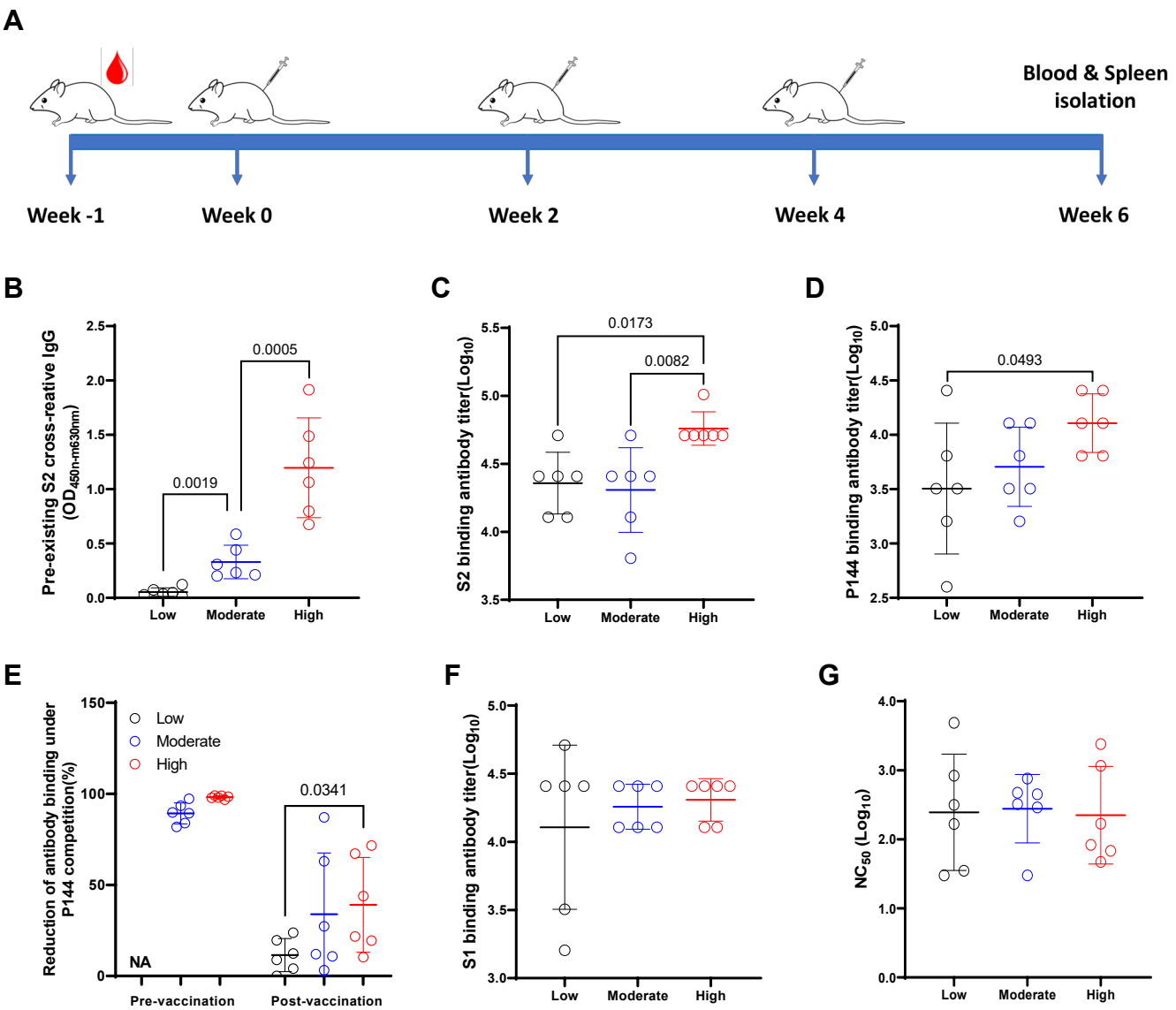

Figure 6. Impact of pre-existing antibodies on the humoral immune responses elicited by a DNA vaccine encoding SARS-CoV-2 S protein. (**A**) Schematic illustration of the vaccination regimen. 50μg of the candidate DNA vaccine was injected intra muscularly into each mice at week 0, week 2 and week 4. Two weeks after the final vaccination, the mice was sacrificed for the measurements of specific immune responses. (**B**) Periphral blood was collected before immunization and levels of pre-existing S2 specific IgG were compared among three groups of mice. (**C**) Comparisons of endpoint IgG titers against S2 in the serum of mice measured at 2 weeks post the last immunization. (**D**) Comparisons of P144 specific IgG titers in the serum of mice as measured using BSA-P144 conjugate as the coating antigen. (**E**) Comparisons of P144 specific binding antibody levels as determined using a method of competitive ELISA. (**F**) Endpoint IgG titers against S1 measured at 2 weeks post the final vaccination. (**G**) Neutralizing antibody titers against SARS-CoV-2 D614G pseudo-virus in serum of mice at 2 weeks post the final immunization. The vaccination experiment was repeated twice with 6 mice for each group. Data were shown as mean±SD. Statistical analyses were performed by the method of one-way ANONVA.

Figure 7

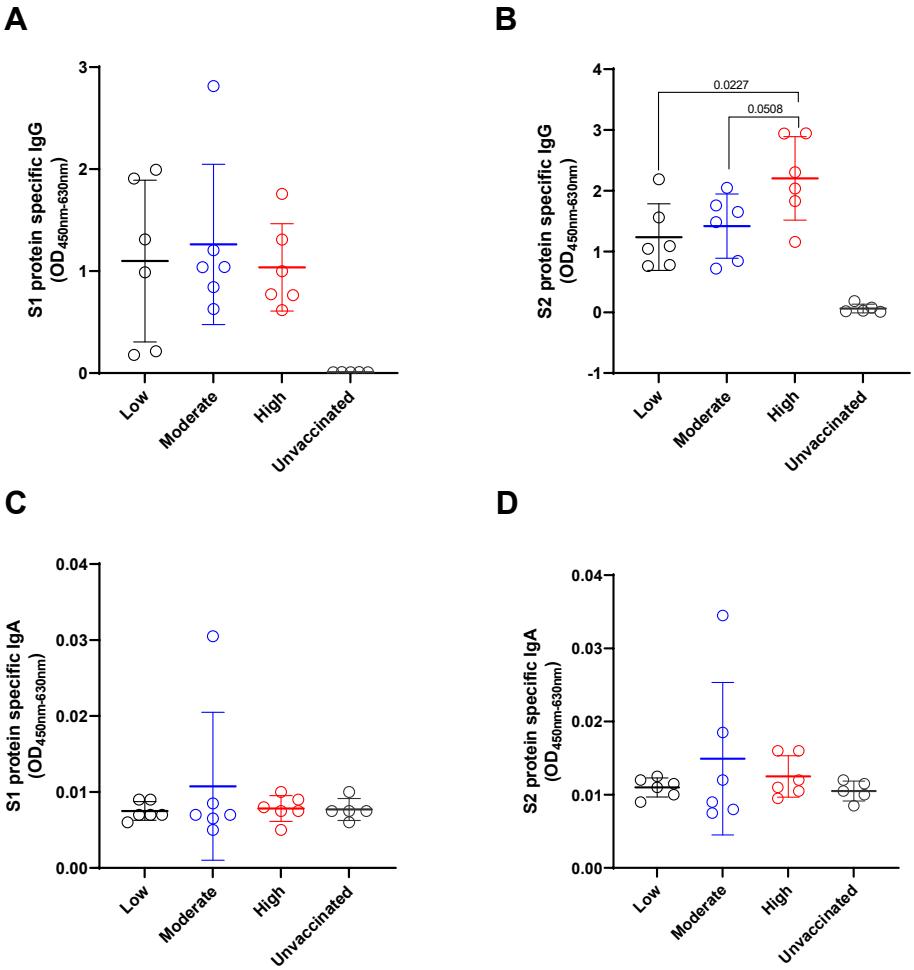

Figure 7. The impact of pre-existing antibody on the levels of specific IgG and IgA in BALF after vaccination. BALF was collected from each mouse after euthanasia. Specific IgG (**A** and **B**) and IgA (**C** and **D**) against S1 or S2 were detected using in-house ELISA methods. All the BALF samples were adjusted to the initial total protein concentration of 51.9μg/ml. Data are shown as mean± SD. Statistical analyses were performed by the method of one-way ANOVA.

Figure 8

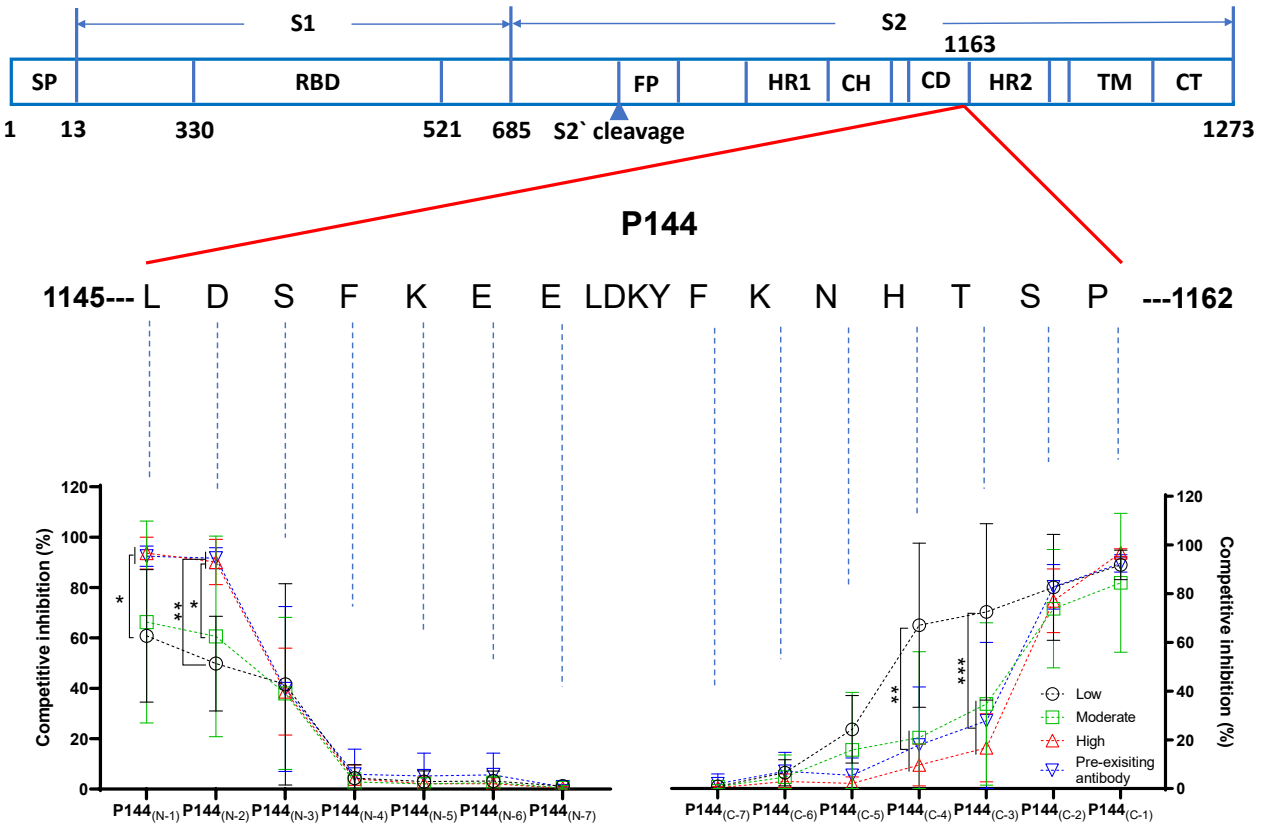

Figure 8. The impact of pre-existing antibody on the minimum epitope recognition of P144 after vaccination. The minimal epitope recognized by mouse sera after vaccination were analyzed using a method of competitive ELISA. Purified BSA-P144 conjugate was used as the coating antigen and truncated peptides derived from P144 were used as the competitors. The decreases of competitive inhibition reflected the necessity of each amino acid for the epitope recognition. Statistical analyses were performed by the method of two-tailed t-test (*, $P< 0.05$, **, $P< 0.01$, ***, $P< 0.001$).

Figure 9

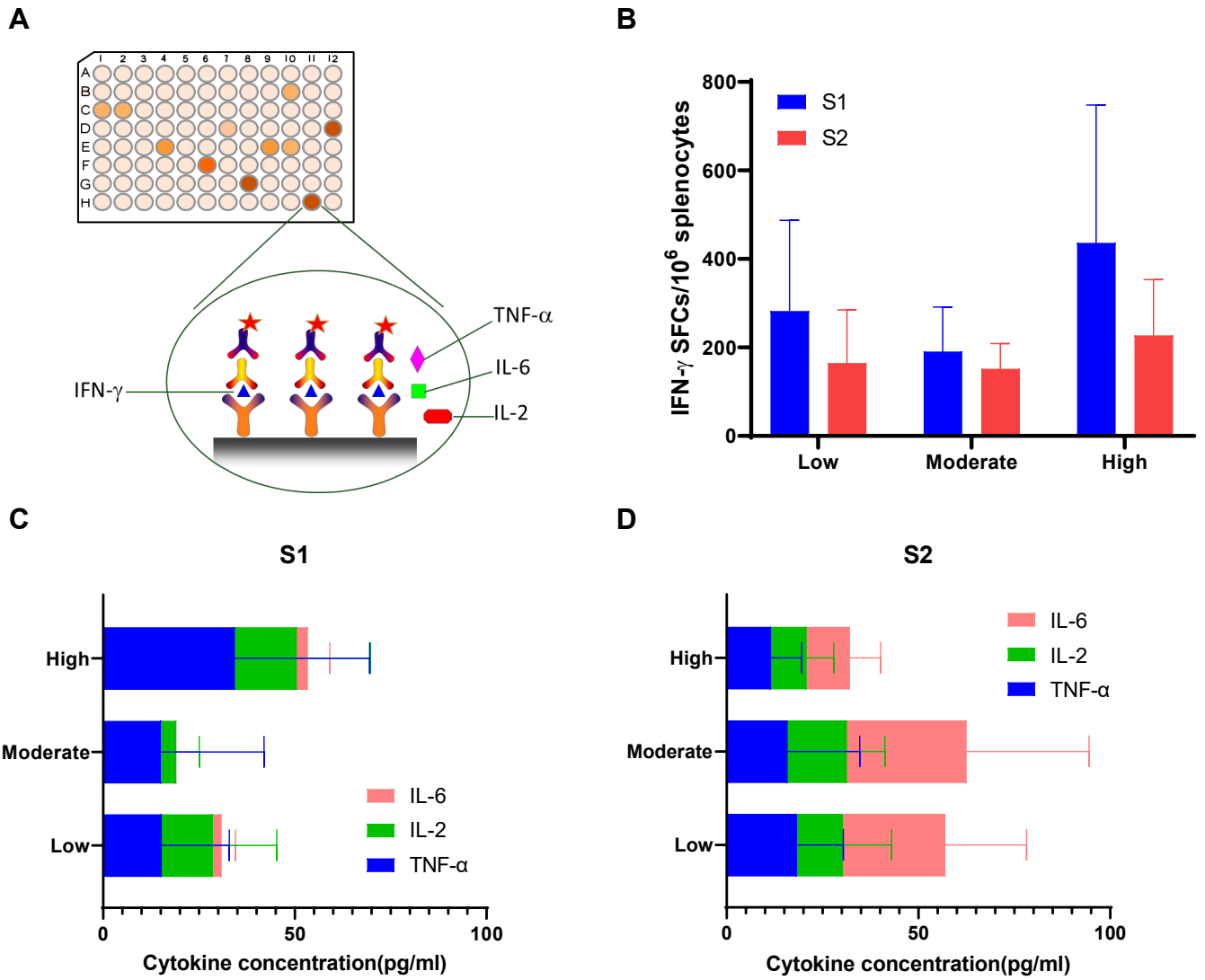

Figure 9. The impact of pre-existing antibody on the cellular immune responses after vaccination. (**A**) The diagram of the method for cellular immune responses assays. (**B**) S1 and S2 specific IFN-γ responses were compared among groups of mice with different levels of pre-existing S2 cross-reactive antibodies. Additionally, S1 (**C**) and S2 (**D**) specific releases of IL-2, IL-6 and TNF-α as measured using the method of multiplex cytokine bead assay were also compared among different groups. Data were shown as mean± SD. SFU, spot forming units.

Figure 10

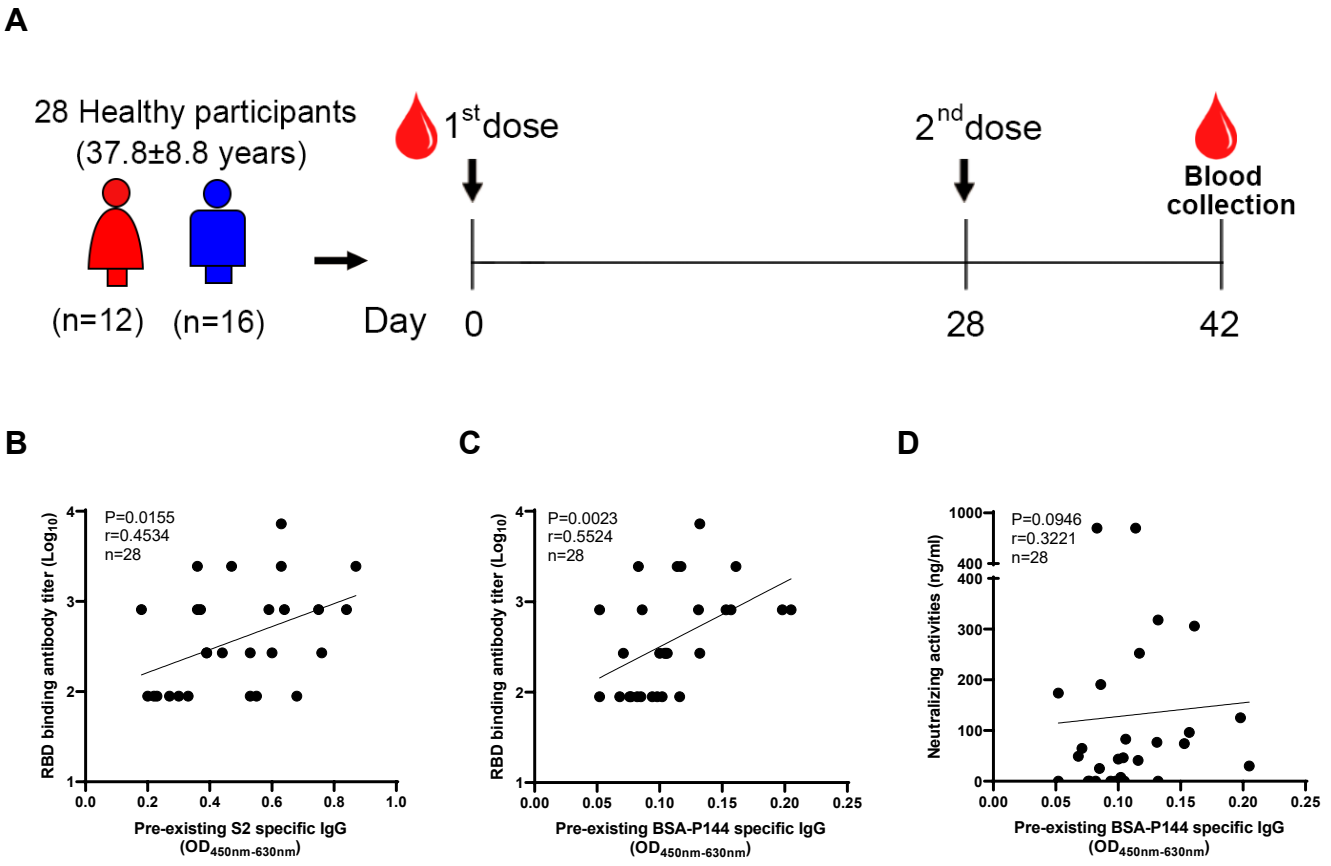

Figure 10. Correlation of pre-existing antibody with RBD and neutralizing activities in healthy individuals vaccinated with inactivated COVID19 vaccine (BBIBP-CorV). (A) 28 healthy individuals were selected and their plasma were collected both before and after vaccinated with inactivated COVID19 vaccine twice. The pre-existing P144 and pre-existing S2 specific antibody were evaluated in plasma before vaccination. The neutralization activities and RBD binding antibody titer were analyzed in plasma after vaccination. **(B and C**) Correlation between RBD binding antibody titer with pre-existing S2 specific IgG or pre-existing BSA-P144 specific IgG. **(D)** Correlation between neutralizing activities with pre-existing BSA-P144 specific IgG. All Correlation was statistically evaluated using Spearman's correlation and linear regression**.**

Table 1 Demographics of SARS-CoV-2 unexposed healthy individuals

Sample Collection Time	**2016**	**2020**
Number of individuals	78	95
Gender (males, females)	17, 61	78, 17
Age, years (mean ± SD)	35.88 ± 8.40	30.40 ± 7.55

Table 2 Potential cross-reactive antigens identified in mouse fecal bacteria

NCBI Accession #	Protein name	Bacterium	Score	Proteins	Unique Peptides	Peptides	PSMs	Area	MW [kDa]
Q8A470	DNA-directed RNA polymerase subunit beta' OS	Bacteroides thetaiotaomicron	168.01	550	2	6	6	3.536E7	158.3
Q5L897	DNA-directed RNA polymerase subunit beta OS	Bacteroides fragilis	92.15	8	2	3	3	8.315E6	142.4
Q8A1G1	TonB-dependent receptor SusC OS	Bacteroides thetaiotaomicron	145.74	1	1	2	3	1.385E8	111.1
Q46509	Aldehyde oxidoreductase OS	Desulfovibrio gigas	75.93	1	1	1	1	8.506E6	97.0
P22983	Pyruvate, phosphate dikinase OS	Clostridium symbiosum	109.83	7	2	2	2	3.721E7	96.6
P0A9Q8	Aldehyde-alcohol dehydrogenase OS	Escherichia coli	34.29	1	1	1	1	1.085E7	96.1
Q826F6	Chaperone protein dnaK2 OS	Streptomyces avermitilis	20.37	1	1	1	1	1.059E7	67.5
Q892R0	Chaperone protein DnaK OS	Clostridium tetani	51.52	5	1	1	1	1.780E7	66.4
B1I9W8	L-fucose isomerase OS	Streptococcus pneumoniae	57.33	12	2	2	2	2.792E7	65.7
P95334	Chaperone protein DnaK OS	Myxococcus xanthus	39.23	4	1	1	1	1.792E7	65.3
Q1MPZ9	Formate--tetrahydrofolate ligase OS	Lawsonia intracellularis	62.49	1	2	2	2	2.068E7	64.2
P26929	Urease subunit alpha OS	Lactobacillus fermentum	134.06	4	4	4	5	1.526E7	61.8
Q9I165	Periplasmic trehalase OS	Pseudomonas aeruginosa	77.05	1	1	1	1	4.240E8	61.1
Q9EZ02	Pyrophosphate--fructose 6-phosphate 1-phosphotransferase OS	Spirochaeta thermophila	68.21	2	1	1	1	1.192E7	61.0
P14407	Fumarate hydratase class I, anaerobic OS	Escherichia coli	30.79	1	1	1	1	6.580E6	60.1
Q189R2	Formate--tetrahydrofolate ligase OS	Clostridioides difficile	123.52	22	3	4	4	2.621E7	59.9
P22252	Flagellin B OS	Campylobacter jejuni subsp. jejuni serotype O:6	75.42	1	1	1	1	1.478E7	59.7
Q1WTW0	Formate--tetrahydrofolate ligase OS	Lactobacillus salivarius	83.43	23	1	1	1	5.229E7	59.4
A7HLZ4	Formate--tetrahydrofolate ligase OS	Fervidobacterium nodosum	93.49	29	1	2	2	8.036E6	59.2
C4ZBL1	Phosphoenolpyruvate carboxykinase (ATP) OS	Agathobacter rectalis	211.34	4	1	4	5	3.965E7	59.0
A6LFQ4	Phosphoenolpyruvate carboxykinase (ATP) OS	Parabacteroides distasonis	32.29	1	1	1	1	8.523E6	58.9
A3MZI4	Formate--tetrahydrofolate ligase OS	Actinobacillus pleuropneumoniae serotype 5b	78.45	78	1	2	2	1.320E8	58.9
Q2LPJ8	60 kDa chaperonin 1 OS	Syntrophus aciditrophicus	101.22	15	1	2	3	2.217E7	58.6
Q3ALZ3	60 kDa chaperonin 1 OS	Synechococcus sp.	113.34	23	1	2	3	9.973E7	58.5
B8J123	60 kDa chaperonin OS	Desulfovibrio desulfuricans	232.59	27	2	5	6	9.659E7	58.4
Q72AL6	60 kDa chaperonin OS	Desulfovibrio vulgaris	126.02	9	1	3	3	2.402E7	58.4

A0Q2T1	60 kDa chaperonin OS	Clostridium novyi	78.78	16	1	2	2	2.292E7	58.1
B0SCC0	60 kDa chaperonin OS	Leptospira biflexa serovar Patoc	49.58	1	1	1	1	1.882E8	58.1
B2TIX0	60 kDa chaperonin OS	Clostridium botulinum	126.34	35	1	3	3	4.903E7	57.9
A7GZ43	60 kDa chaperonin OS	Campylobacter curvus	105.05	41	2	3	3	5.327E7	57.9
Q67KB8	60 kDa chaperonin OS	Symbiobacterium thermophilum	107.47	126	1	3	3	9.411E7	57.9
B5YDR9	60 kDa chaperonin OS	Dictyoglomus thermophilum	59.61	2	1	1	1	3.345E7	57.9
Q3ADX3	60 kDa chaperonin OS	Carboxydothermus hydrogenoformans	104.07	25	1	2	3	7.715E7	57.6
O50305	60 kDa chaperonin OS	Bacillus halodurans	250.57	55	3	4	6	3.021E8	57.4
P26821	60 kDa chaperonin OS	Clostridium perfringens	131.27	36	1	3	3	4.609E7	57.3
P37282	60 kDa chaperonin OS	Lactococcus lactis subsp. lactis	102.15	18	1	2	2	4.298E7	57.2
C4ZD46	60 kDa chaperonin OS	Agathobacter rectalis	372.10	52	3	5	8	3.352E8	57.1
A6L8C4	Glucose-6-phosphate isomerase OS	Parabacteroides distasonis	88.85	55	1	2	3	5.392E8	48.7
P43793	NADP-specific glutamate dehydrogenase OS	Haemophilus influenzae	96.32	2	1	2	2	7.357E7	48.6
P00370	NADP-specific glutamate dehydrogenase OS	Escherichia coli	161.88	1	1	3	4	3.280E8	48.6
P15111	NADP-specific glutamate dehydrogenase OS	Salmonella typhimurium	185.28	4	1	4	5	1.755E8	48.5
P94316	NAD-specific glutamate dehydrogenase OS	Bacteroides fragilis	192.93	3	3	5	6	1.730E8	48.4
Q1WSY0	Enolase OS	Lactobacillus salivarius	79.89	8	3	3	3	1.340E7	48.0
B7MD95	Trigger factor OS	Escherichia coli O45:K1	78.80	10	2	2	2	4.344E7	47.8
B2GAM0	Enolase OS	Lactobacillus fermentum	79.94	8	2	2	2	1.858E7	47.8
Q6MEY2	Enolase OS	Protochlamydia amoebophila	112.67	1	1	1	1	7.493E7	47.5
Q0SNH5	Enolase OS	Borrelia afzelii	71.86	2	1	1	1	4.654E7	47.4
G3KIM4	Lactoyl-CoA dehydratase subunit alpha (Fragment) OS	Anaerotignum propionicum	63.03	1	1	1	1	1.136E7	47.4
Q9I3S1	Biofilm dispersion protein BdlA OS	Pseudomonas aeruginosa	59.07	22	1	1	1	3.282E7	46.9
B8J4A8	Sulfate adenylyltransferase OS	Desulfovibrio desulfuricans	210.65	1	5	5	5	2.656E7	46.9
A6L3M9	Enolase OS	Bacteroides vulgatus	48.62	2	1	2	2	3.004E7	46.7
Q043Z5	Enolase 1 OS	Lactobacillus gasseri	289.72	4	5	5	5	4.189E7	46.6
Q1ISS7	Enolase OS	Koribacter versatilis	71.57	4	1	1	1	7.884E6	46.5
B8DTI9	Enolase OS	Bifidobacterium animalis subsp. lactis	115.71	4	2	2	2	1.684E7	46.4
A7GUR7	Enolase OS	Bacillus cytotoxicus	122.68	17	2	2	3	2.771E7	46.4
Q2LR33	Enolase OS	Syntrophus aciditrophicus	31.73	1	1	1	1	4.823E7	46.2
Q89Z05	Enolase OS	Bacteroides thetaiotaomicron	140.16	2	2	4	5	3.005E7	46.1

B2RLL7	Enolase OS	Porphyromonas gingivalis	123.91	2	2	3	3	2.636E7	45.8
Q6MPQ2	Enolase OS	Bdellovibrio bacteriovorus	66.50	1	1	1	1	8.918E6	45.7
B0K742	Serine hydroxymethyltransferase OS	Thermoanaerobacter pseudethanolicus	85.67	92	2	2	2	2.140E7	45.6
Q5LFT7	Peptidase T OS	Bacteroides fragilis	89.56	5	1	1	1	7.323E7	45.5
A9NEA9	Serine hydroxymethyltransferase OS	Acholeplasma laidlawii	44.82	3	1	1	1	5.875E6	45.3
Q7MU77	Phosphoglycerate kinase OS	Porphyromonas gingivalis	54.70	1	1	1	1	2.106E7	45.0
Q8A753	Phosphoglycerate kinase OS	Bacteroides thetaiotaomicron	25.30	1	1	1	1	1.320E7	45.0
A5VHR0	Phosphopentomutase OS	Lactobacillus reuteri	159.08	1	4	4	4	4.364E7	44.0
A8EWM4	Phosphoglycerate kinase OS	Arcobacter butzleri	45.52	1	1	1	1	2.577E7	43.8
Q042T5	Elongation factor Tu OS	Lactobacillus gasseri	400.92	36	3	10	13	1.184E8	43.7
Q74JU6	Elongation factor Tu OS	Lactobacillus johnsonii	348.06	36	2	9	12	1.184E8	43.6
Q5L890	Elongation factor Tu OS	Bacteroides fragilis	185.88	297	3	5	7	1.454E8	43.6
Q8R603	Elongation factor Tu OS	Fusobacterium nucleatum subsp. nucleatum	150.02	302	1	3	3	6.170E7	43.4
B8J1A0	Elongation factor Tu OS	Desulfovibrio desulfuricans	139.50	64	2	3	3	4.287E7	43.4
A5VJ92	Elongation factor Tu OS	Lactobacillus reuteri	413.79	60	8	11	13	3.595E8	43.4

Note: *Score:* The Mascot score. Proteins: The total number of proteins contained in the protein group. *Unique Peptides:* The total number of peptides unique to the protein group. *Peptides:* The total number of peptides identified from all included searches for the master protein of the protein group. *PSMs:* The total number of peptide-spectrum matches identified from all included searches for the master protein of the protein group. *Area:* The chromatographic peak area was used to characterize the quantitative abundance of protein.*MW(kDa):* The theoretical molecular weight of the protein.

Table 3 Potential cross-reactive antigens identified in human fecal bacteria

NCBI Accession #	Protein Name	Bacterium	Score	Proteins	Unique Peptides	Peptides	PSMs	Area	MW [kDa]
A6LFK9	Polyribonucleotide nucleotidyltransferase OS	Parabacteroides distasonis	62.68	3	1	2	2	2.332E7	82.0
P75764	Uncharacterized protein YbhJ OS	Escherichia coli	27.35	1	1	1	1	3.198E7	81.5
Q8A4N6	Polyribonucleotide nucleotidyltransferase OS	Bacteroides thetaiotaomicron	226.97	23	6	7	7	6.947E7	78.3
B3DT30	Elongation factor G OS	Bifidobacterium longum	236.98	64	8	10	11	4.407E7	78.1
E1WNR6	Chaperone protein htpG OS	Bacteroides fragilis	131.15	4	1	2	2	4.992E7	77.9
O31673	ATP-dependent Clp protease ATP-binding subunit ClpE OS	Bacillus subtilis	120.19	73	1	3	4	8.448E7	77.9
A7ZSL5	Elongation factor G OS	Escherichia coli O139:H28	133.81	92	2	3	4	2.888E7	77.5
Q5L8A7	Elongation factor G OS	Bacteroides fragilis	431.35	187	3	10	14	1.391E8	77.5
A6KYJ7	Elongation factor G OS	Bacteroides vulgatus	361.61	186	2	9	12	1.342E8	77.4
A6LFP0	Methionine--tRNA ligase OS	Parabacteroides distasonis	65.86	8	1	1	1	4.772E7	77.4
P39396	Pyruvate/proton symporter BtsT OS	Escherichia coli	92.20	1	2	2	2	1.446E7	77.3
A9KNK6	Polyribonucleotide nucleotidyltransferase OS	Lachnoclostridium phytofermentans	68.87	1	1	1	1	1.075E8	76.9
Q5L6S5	Elongation factor G OS	Chlamydia abortus	76.05	58	1	2	3	1.622E7	76.8
Q67JU0	Elongation factor G OS	Symbiobacterium thermophilum	147.39	86	1	4	5	2.631E8	76.8
Q5U8S9	Elongation factor G OS	Staphylococcus intermedius	98.88	65	1	3	4	5.177E7	76.7
Q8A294	Putative K(+)-stimulated pyrophosphate-energized sodium pump OS	Bacteroides thetaiotaomicron	150.65	20	1	3	3	1.276E8	76.5
B9DYA6	Elongation factor G OS	Clostridium kluyveri	136.00	67	1	3	4	8.826E7	76.4
Q5WLR5	Elongation factor G OS	Bacillus clausii	134.85	81	1	4	5	1.119E8	76.4
Q97I51	Translation initiation factor IF-2 OS	Clostridium acetobutylicum	70.53	4	1	1	1	2.330E8	76.3
A0PXU3	Elongation factor G OS	Clostridium novyi	114.21	67	1	3	4	8.905E7	76.1
Q18CF4	Elongation factor G OS	Clostridioides difficile	174.49	59	1	4	5	1.288E8	75.8
Q8AB53	Putative glucosamine-6-phosphate deaminase-like protein BT_0258 OS	Bacteroides thetaiotaomicron	54.10	1	1	1	1	4.629E6	75.2
Q8XJ01	Penicillin-binding protein 1A OS	Clostridium perfringens	39.66	3	1	1	1	1.599E7	75.1
A6L7J7	Threonine--tRNA ligase OS	Bacteroides vulgatus	91.33	9	2	2	2	2.440E7	74.2
P30539	1,4-alpha-glucan branching enzyme GlgB OS	Butyrivibrio fibrisolvens	30.12	1	1	1	1	2.287E7	73.8
B2TIT5	Threonine--tRNA ligase OS	Clostridium botulinum	53.61	2	1	1	1	1.877E7	73.8

P56116	Chaperone protein HtpG OS	Helicobacter pylori	38.02	12	1	1	1	1.269E7	71.2
P0A9P7	ATP-dependent RNA helicase DeaD OS	Escherichia coli O6:H1	85.88	5	3	3	4	1.336E8	70.5
P19410	3-oxocholoyl-CoA 4-desaturase OS	Clostridium scindens	63.87	1	1	1	1	5.844E7	70.2
Q8RHJ2	Putative K(+)-stimulated pyrophosphate-energized sodium pump OS	Fusobacterium nucleatum subsp. nucleatum	140.41	23	1	3	3	1.320E8	68.9
A5CX56	Chaperone protein DnaK OS	Vesicomyosocius okutanii subsp. Calyptogena okutanii	15.38	1	1	1	1	2.961E7	68.7
Q5LG30	Chaperone protein DnaK OS	Bacteroides fragilis	418.39	33	1	9	11	6.399E7	68.6
Q89YW6	Chaperone protein DnaK OS	Bacteroides thetaiotaomicron	372.24	35	1	7	9	6.399E7	68.3
A6L2X7	Chaperone protein DnaK OS	Bacteroides vulgatus	371.71	33	1	8	10	6.399E7	68.3
Q93GF1	Chaperone protein DnaK OS	Prevotella loescheii	185.46	1	4	4	4	3.512E7	68.0
A6LGR5	4-hydroxy-3-methylbut-2-en-1-yl diphosphate synthase (flavodoxin) OS	Parabacteroides distasonis	38.34	5	1	1	1	2.396E7	67.9
B8H444	ATP-dependent zinc metalloprotease FtsH OS	Caulobacter vibrioides	26.45	6	1	1	1	1.241E7	67.7
A9KIA6	Aspartate--tRNA(Asp/Asn) ligase OS	Lachnoclostridium phytofermentans	31.12	1	1	1	1	8.400E6	67.5
P0AG91	Protein translocase subunit SecD OS	Escherichia coli O157:H7	233.70	2	6	6	6	2.164E7	66.6
Q49Y22	Chaperone protein DnaK OS	Staphylococcus saprophyticus subsp. saprophyticus	56.64	206	1	2	2	1.171E7	66.5
A6LBU6	Aspartate--tRNA ligase OS	Parabacteroides distasonis	88.06	49	1	2	2	7.901E6	66.4
P21332	Oligo-1,6-glucosidase OS	Bacillus cereus	53.99	2	1	1	1	1.391E7	66.0
Q8A5W4	Lysine--tRNA ligase OS	Bacteroides thetaiotaomicron	154.84	2	2	2	2	1.304E7	65.9
Q8GBW6	Methylmalonyl-CoA carboxyltransferase 12S subunit OS	Propionibacterium freudenreichii subsp. shermanii	98.01	1	1	1	2	1.386E8	65.9
Q67S54	Chaperone protein DnaK OS	Symbiobacterium thermophilum	96.29	225	1	3	3	4.528E7	65.7
Q9RQ13	L-fucose isomerase OS	Bacteroides thetaiotaomicron	181.20	7	1	5	7	1.038E8	65.7
A6L048	L-fucose isomerase OS	Bacteroides vulgatus	162.35	5	2	6	7	3.672E7	65.6
Q56403	V-type ATP synthase alpha chain OS	Thermus thermophilus	132.50	30	1	1	2	1.117E7	63.6
Q8G7I6	Glucose-6-phosphate isomerase OS	Bifidobacterium longum	531.07	4	14	14	15	3.155E8	63.0
Q4JX51	Glucose-6-phosphate isomerase OS	Corynebacterium jeikeium	30.85	1	1	1	1	3.306E7	62.1
Q8FZC4	2-isopropylmalate synthase OS	Brucella suis biovar 1	51.65	8	1	1	1	1.014E7	61.6
A6TGT4	Glucose-6-phosphate isomerase OS	Klebsiella pneumoniae subsp. pneumoniae	53.60	21	1	1	1	3.337E7	61.3

P0AG69	30S ribosomal protein S1 OS	Escherichia coli O157:H7	88.52	1	2	2	2	8.393E6	61.1
Q9EZ02	Pyrophosphate--fructose 6-phosphate 1-phosphotransferase OS	Spirochaeta thermophila	110.07	2	2	2	2	1.245E8	61.0
O31716	Uncharacterized ABC transporter ATP-binding protein YkpA OS	Bacillus subtilis	48.45	1	1	1	1	2.259E6	61.0
P59173	Probable 2,3-bisphosphoglycerate-independent phosphoglycerate mutase OS	Leptospira interrogans serogroup Icterohaemorrhagiae serovar Lai	61.50	2	1	1	2	6.104E6	61.0
P23843	Periplasmic oligopeptide-binding protein OS	Escherichia coli	368.94	2	11	11	12	1.586E8	60.9
Q0SQ82	Formate--tetrahydrofolate ligase OS	Clostridium perfringens	167.47	26	1	3	4	6.063E7	60.4
P14407	Fumarate hydratase class I, anaerobic OS	Escherichia coli	66.46	4	2	2	2	4.922E7	60.1
Q3A9K2	Formate--tetrahydrofolate ligase OS	Carboxydothermus hydrogenoformans	110.68	55	1	3	3	3.356E8	60.1
Q251P8	Formate--tetrahydrofolate ligase 1 OS	Desulfitobacterium hafniense	72.85	55	1	2	2	5.742E8	60.0
C0QX38	Formate--tetrahydrofolate ligase OS	Brachyspira hyodysenteriae	145.04	9	1	2	3	2.562E7	60.0
Q189R2	Formate--tetrahydrofolate ligase OS	Clostridioides difficile	157.46	1	3	3	3	1.347E9	59.9
C4ZBG8	Formate--tetrahydrofolate ligase OS	Agathobacter rectalis	235.86	56	4	6	6	3.610E8	59.7
A8AQV7	Phosphoenolpyruvate carboxykinase (ATP) OS	Citrobacter koseri	104.30	44	4	5	5	1.300E8	59.6
Q24ZZ8	Formate--tetrahydrofolate ligase 2 OS	Desulfitobacterium hafniense	79.67	55	1	2	2	5.193E8	59.4
B2RHV8	Phosphoenolpyruvate carboxykinase (ATP) OS	Porphyromonas gingivalis	188.39	21	2	5	5	2.446E8	59.4
Q47VD0	Phosphoenolpyruvate carboxykinase (ATP) OS	Colwellia psychrerythraea	111.53	16	1	2	2	1.952E8	59.3
A1R7X2	Arginine--tRNA ligase OS	Paenarthrobacter aurescens	43.93	15	1	1	1	2.994E7	59.2
Q8A414	Phosphoenolpyruvate carboxykinase (ATP) OS	Bacteroides thetaiotaomicron	293.03	21	3	8	8	3.939E8	59.1
C4ZBL1	Phosphoenolpyruvate carboxykinase (ATP) OS	Agathobacter rectalis	501.52	17	5	12	15	4.167E8	59.0
Q5L7N5	Phosphoenolpyruvate carboxykinase (ATP) OS	Bacteroides fragilis	420.91	17	1	6	12	2.103E8	59.0
A3CL27	Formate--tetrahydrofolate ligase 1 OS	Streptococcus sanguinis	145.32	20	1	2	3	3.296E7	59.0
A6LFQ4	Phosphoenolpyruvate carboxykinase (ATP) OS	Parabacteroides distasonis	438.19	17	5	11	14	2.336E8	58.9
C4ZAW6	Dihydroxy-acid dehydratase OS	Agathobacter rectalis	193.87	6	5	6	6	2.765E7	58.9
B9E299	Dihydroxy-acid dehydratase OS	Clostridium kluyveri	85.82	2	1	2	3	7.244E7	58.8
O09460	Phosphoenolpyruvate carboxykinase (ATP) OS	Anaerobiospirillum succiniciproducens	214.42	21	2	5	5	3.702E8	58.6
B2TIR2	Dihydroxy-acid dehydratase OS	Clostridium botulinum	46.21	2	1	1	1	3.131E6	58.5
B3DTV2	ATP synthase subunit alpha OS	Bifidobacterium longum	383.31	393	9	11	12	5.746E7	58.4
B3DRY6	Bifunctional purine biosynthesis protein PurH OS	Bifidobacterium longum	204.27	2	3	3	3	1.243E8	58.4
A6LIG0	60 kDa chaperonin OS	Parabacteroides distasonis	325.96	2	1	7	10	4.117E8	58.3

A5N857	Ribonuclease Y OS	Clostridium kluyveri	85.68	95	1	3	3	4.874E7	58.3
Q8G3N6	Inosine-5'-monophosphate dehydrogenase OS	Bifidobacterium longum	685.57	20	15	16	19	2.005E8	58.2
Q8A6P8	60 kDa chaperonin OS	Bacteroides thetaiotaomicron	591.81	1	2	11	15	2.794E8	58.2
Q5LAF6	60 kDa chaperonin OS	Bacteroides fragilis	690.75	1	4	15	20	5.301E8	58.2
A0Q2T1	60 kDa chaperonin OS	Clostridium novyi	58.42	6	2	2	2	2.212E8	58.1
A6KXA0	60 kDa chaperonin OS	Bacteroides vulgatus	948.24	1	11	22	26	6.146E8	58.1

Note: *Score:* The Mascot score. Proteins: The total number of proteins contained in the protein group. *Unique Peptides:* The total number of peptides unique to the protein group. *Peptides:* The total number of peptides identified from all included searches for the master protein of the protein group. *PSMs:* The total number of peptide-spectrum matches identified from all included searches for the master protein of the protein group. *Area:* The chromatographic peak area was used to characterize the quantitative abundance of protein. *MW(kDa):* The theoretical molecular weight of the protein.